Development of Breathable, Self-Sealing Protective Garment

by

Aastha Uppal

A Thesis Presented in Partial Fulfillment
of the Requirements for the Degree
Master of Science

Approved April 2016 by the
Graduate Supervisory Committee:

Konrad Rykaczewski, Chair
Owen Hildreth
Hamidreza Marvi

ARIZONA STATE UNIVERSITY

May 2016

ABSTRACT

"Smart" materials are used for a broad range of application including electronics, bio-medical devices, and smart clothing. This work focuses on development of smart self-sealing and breathable protective gear for soldiers against Chemical Weapon Agents (CWA). Specifically, the response of chemo-mechanical swelling polymer modified meshes to contact with stimuli droplets was studied. Theoretical discussion of the mechanism of smart materials is followed by development and experimental analysis of different modified mesh designs. A multi-physics model is proposed based on experimental data and the prototype of the fabric is tested in aerosol impingement conditions to confirm the barrier formed by rapid-self-sealing feature of the design.

TABLE OF CONTENTS

Page

CHAPTER Page

LIST OF TABLES

Table Page

LIST OF FIGURES

Figure Page

Figure Page

1. INTRODUCTION

Mission Oriented Protective Posture (MOPP) apparel is required to protect the soldiers against biological and chemical weapon agents (CWA) as exposure to even minute amount of these toxins can be fatal. Currently MOPP consists of poreless polymer coatings that form an impermeable barrier to the transport of harmful toxins. The major drawback of this MOPP design is that it also inhibits transport of moisture and hence prevents evaporative cooling through sweating [1]. This increases the thermal load on a soldier and hence safe usage of the gear is restricted to about 1 hour in moderate climate. In more severe conditions such as the middle-east that can experience significant solar loads and ambient temperatures above 130 F, this time limit is further reduced [2]. Specialized garments with cooling provided by phase change material or active fluid pumping are necessary for prolonged usage [3]. The addition of the cooling system increases the size, weight, complexity, and cost of the protective gear. In addition, operation of the cooling systems can have additional requirements such as batteries for the pump or refrigerator to pre-freeze the phase change material. Putting all factors together, regular MOPP gear use is limited to a short time period due to inhibited evaporative cooling, while more specialized garments with cooling system might not be readily available in the field conditions.

An improved and more efficient design is proposed as a solution to the above issues. In particular, the development of a smart self-sealing and breathable protective gear is proposed. As illustrated in Figure 1.1, the fabric will be breathable in normal conditions

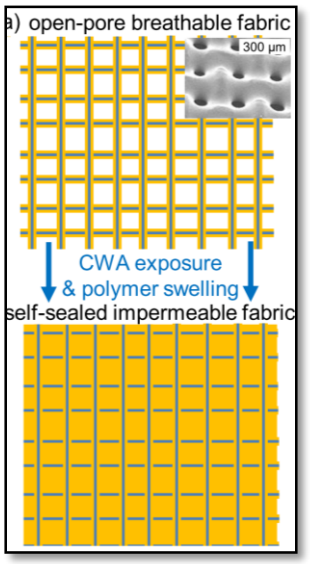

Figure 1.1 Schematic of the Proposed Mechanism of Self-Sealing and Breathable Fabric.

and will form an impermeable barrier when it comes in contact with a wide range of CWAs. This is based on the chemo-responsive Shape Change Polymers (SCPs) that are widely used in smart apparels and fibers for applications in the medical, sports, and textile industries [4]. Proof-of-concept experiments are conducted using PDMS as the polymer responding to organic solvents by swelling and hence demonstrating closing of open pores. Efficiency and effectiveness of the self-sealed impermeable membrane is improved by developing optimal design using a superabsorbing polymer as well as its PDMS composite. The mechanism of self-sealing is studied experimentally and influence of the design factors on the formation of barrier and rate of self-sealing is discussed. The work concludes by highlighting the main features of the design and how these protocols can be used to develop a design with novel elastomers which are responsive to CWAs and design breathable, self-sealing and self-decontaminating protective gear.

2. SMART MATERIALS: SELF-CLEANING SURFACES AND SELF-SEALING MATERIALS

2.1 Self-Cleaning Surfaces

One of the issues that arises with use of traditional polymer barriers is potential contamination of the material with the CWA via absorption and its potential release outside of the direct exposure zone. Since exposure to even a minute amount of CWA such as sarin can be deadly, delayed release of absorbed CWA is highly undesired. In turn, the Ebola crisis provides a recent example of how contamination of personal protective equipment (PPE) with a biological hazard in liquid form can pose challenges. In particular, numerous medical staff were exposed to the virus in the early stages of the disease spread due to limited supply of single use PPE such as gloves and aprons. As a last resort, the existing PPE was often cleaned and reused, but often with questionable effectiveness.

Both of these challenges could be addressed by development of PPE that can repel all the liquids which come in contact with it. Such omniphobic surfaces can be created with use of low surface energy treatments and addition of re-entrant nano/micro-texture. However, such fabrics could be penetrated by most CWAs because they are dispersed in aerosol form with microdroplets that are of comparable size to the surface microtexture. This issue can be resolved by infusion of a low vapor pressure lubricant into the texture. The so-called slippery lubricant infused porous surfaces (SLIPS) can have self-cleaning, self-healing, and pressure tolerant characteristics. The self-healing mechanism is achieved because the liquid flows to the damaged area due to capillary action [5]. However, it was shown that the lubricant can easily wick away from nano-textured fabric fibers upon contact with an external porous material, such as a paper towel. To address this durability

issue, SLIPS fabrics consisting of lubricant swollen polymers (e.g. PDMS swollen with silicone oil) were developed [6].

While useful in many applications, the self-cleaning SLIPS based PPE is also a barrier to moisture transport. The protective gear design proposed in this thesis aims at being breathable with micro/nano openings which will self-seal when exposed to CWA drops. Once the CWA is absorbed into the material, incorporation of a military grade activated carbon is proposed in order to chemically decompose the CWA into more benign products that are not harmful to humans. The rest of this chapter focusses on description of smart materials that could be used to fabricate such fabrics.

2.2 Stimuli Responsive Polymers (SRPs)

Stimuli Response materials commonly known as smart materials have varied applications and are often inspired by natural phenomena [4]. For example, shutting of the Venus Flytrap plant leaves in order to capture insects [4] [7], the closing of leaves by plant Mimosa Pudica in response to touch, and turning of the Sunflower towards sunlight are a few commonly observed stimuli response mechanisms which have inspired the development of novel devices using SRPs [4]. The smart synthetic materials can be broadly characterized as having an ability to modify their physical and chemical properties upon exposure to the target stimuli [8]. The stimuli can be a change in external moisture [9] [10], temperature [9] [8] [11] [12], pH value [13] [14], solvent concentration [4] [15], and mechanical load [12]. The pre-determination of the extent and the particular characteristic of the SRP that will be modified in response to the target stimuli makes them useful in developing novel system designs [8]. Section 2.3 reviews the mechanism of Shape Change

Effect and Shape Memory Effect, while section 2.4 describes mechanism of shape change in response to chemical stimulus (chemo-mechanical effect).

2.3 Shape Change Effect (SCE) and Shape Memory Effect (SME) Mechanisms

Stimuli Response Polymers (SRPs) are categorized as thermo-responsive (heating/cooling), chemo-responsive (chemical including water), photo-responsive (light), and mechano-responsive (mechanical load) [8] [16] [17]. Typically there are two kinds of response that can be observed to these stimuli: Shape Change Effect (SCE) and Shape Memory Effect (SME). The difference in these effects is attributed to the energy barrier the material has to overcome to switch from one state (e.g. deformed) to the other state (e.g. undeformed or original). In the Shape Change Effect the energy barrier is very low and upon removal of the external stimulus the material returns to its original state without the use of any other external stimulus [8] [16]. Retention of the deformed state by the material upon removal of the external stimulus results in the Shape Memory Effect (SME). In this case the material remains in the deformed state unless an additional external stimulus is applied to help it cross the high energy barrier. An intermediate case exists where the energy barrier is low and hence the material returns to its original shape gradually. Figure 2.1 below explains all the three energy barriers (zero energy barrier-SCE, high energy barrier H and low energy barrier H'-SME) [16] [18]).

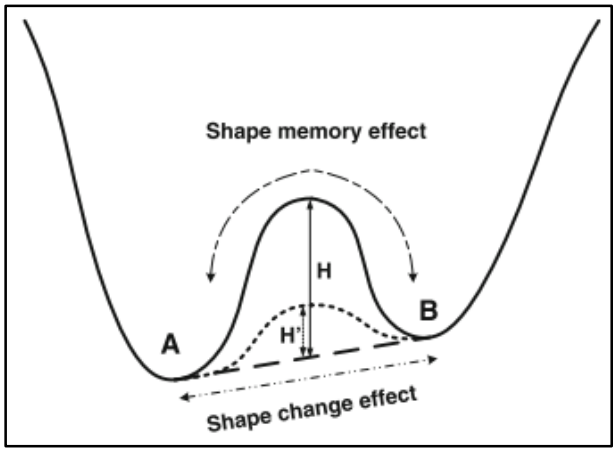

Figure 2.1 Shape Change Effect (SCE) and Shape Memory Effect (SME) Based on Energy Barrier to be Crossed by Any Material to go From State A to B [16].

In order to develop a breathable, self-sealing design for the military protective gear against Chemical Warfare Agents (CWAs), the selected materials should show Chemo-responsive Shape Change Effect (SCE). Hence the mechanism of Chemo-responsive Shape Change polymers is discussed in detail in the next section.

2.4 Chemo-Responsive Shape Change Polymers (SCPs)

Chemo-responsive Shape Change Polymers (SCPs) are composed of an elastic network of molecules that get deformed when exposed to the target chemical stimulus. This process results in temporary change in shape of the polymer [18] and is driven by the transport of the stimuli chemical within the material, not a chemical reaction [19]. The chemo-response of SCPs is typically categorized by the degree of swelling as limited swelling (reversible), significant swelling (reversible), and infinite swelling (diffusion-irreversible) [19]. In the limited swelling case, a small amount of solvent penetrates inside the polymer and insignificant deformation occurs. In the significant swelling case, the polymer undergoes a

high volume expansion because significant amount of solvent penetrates the polymer. The infinite swelling case occurs when diffusion dominates the chemical transport process. The solvent penetrates the polymer until a concentration gradient exists. Mass diffusion is governed by Fick's law of diffusion which states that the flux '*Q*' (in mol/m^{2}s) is proportional to the concentration gradient (*dc/dx*) in the direction of flow with '*D*' as the diffusion coefficient [20].

$$Q = -D\frac{dc}{dx} \tag{2.1}$$

In the current thesis we use two liquid and polymer pairs to explore the relationship between the droplet impact, liquid diffusion in the solid, and swelling dynamics of the polymer coated on open pore mesh. The next section briefly discusses one of the polymers identified to be used for conducting proof-of-concept experiments.

2.5 Solvent Compatibility and Swelling Ratio of Polydimethylsiloxane (PDMS)

Polydimethylsiloxane (PDMS) was selected as one of the polymers to be used for the proof-of-concept experiments exploring the relationship between swelling ratio and pore diameter change due to the polymers' high swelling ratio to organic solvents. This section reviews the swelling characteristic of PDMS with common organic solvents.

PDMS is widely used to make microfluidic devices. Swelling of the polymer in these applications is undesirable as it can result in blockage of the micro channels [21] [22]. The degree of swelling has been experimentally determined by measuring the ratio of the mass of the swollen PDMS and solvent to the mass of the dry PDMS [22]. The most compatible organic solvents which result in least swelling are the ones which have low solubility in PDMS [21]. The rate of swelling obtained for various solvents has been reported over a

period of 24 hours to understand the exposure time required to obtain maximum swelling effect [23].

Solvent compatibility takes into account the behavior of polymer with a given solvent in terms of solubility and swelling ratio [21] [22]. Table 2.1 [21] illustrates the solubility parameter δ ($cal^{\frac{1}{2}}cm^{\frac{-3}{2}}$), experimentally measured swelling ratio S, dipole moment of solvent μ (D), literature values of δ and μ as ref [c] and order of solvent in decreasing swelling ability rank[d].

Table 2.1 PDMS-Solvent Compatibility Parameters and Relationship Between Swelling Ratio and Solubility Parameter for Various Solvents with '1' Having the Maximum Swelling Ability

solvent	δ[a]	S[b]	μ (D)	ref[c]	rank[d]
perfluorotributylamine	5.6	1.00	0.0	10	32
perfluorodecalin	6.6	1.00	0.0	10	33
pentane	7.1	1.44	0.0	10	3
poly(dimethylsiloxane)	7.3	∞	0.6–0.9	8, 14	
diisopropylamine	7.3	2.13	1.2	10	1
hexanes	7.3	1.35	0.0	10	8
n-heptane	7.4	1.34	0.0	10	10
triethylamine	7.5	1.58	0.7	8,10	2
ether	7.5	1.38	1.1	10	6
cyclohexane	8.2	1.33	0.0	10	11
trichloroethylene	9.2	1.34	0.9	10	9
dimethoxyethane (DME)	8.8	1.32	1.6	10	12
xylenes	8.9	1.41	0.3	10	4
toluene	8.9	1.31	0.4	10	13
ethyl acetate	9.0	1.18	1.8	8,10	19
benzene	9.2	1.28	0.0	10	14
chloroform	9.2	1.39	1.0	10	5
2-butanone	9.3	1.21	2.8	10	18
tetrahydrofuran (THF)	9.3	1.38	1.7	10	7
dimethyl carbonate	9.5	1.03	0.9	8,10	25
chlorobenzene	9.5	1.22	1.7	10	15
methylene chloride	9.9	1.22	1.6	10	16
acetone	9.9	1.06	2.9	8,12	22
dioxane	10.0	1.16	0.5	10	20
pyridine	10.6	1.06	2.2	10	23
N-methylpyrrolidone (NMP)	11.1	1.03	3.8	10	26
tert-butyl alcohol	10.6	1.21	1.6	8,12	17
acetonitrile	11.9	1.01	4.0	10	31
1-propanol	11.9	1.09	1.6	8,10	21
phenol	12.0	1.01	1.2	8,12	29
dimethylformamide (DMF)	12.1	1.02	3.8	8,10	27
nitromethane	12.6	1.00	3.5	10	34
ethyl alcohol	12.7	1.04	1.7	8,12	24
dimethyl sulfoxide (DMSO)	13.0	1.00	4.0	10	35
propylene carbonate	13.3	1.01	4.8	10	30
methanol	14.5	1.02	1.7	8,12	28
ethylene glycol	14.6	1.00	2.3	8,12	36
glycerol	21.1	1.00	2.6	13,15	37
water	23.4	1.00	1.9	8,12	38

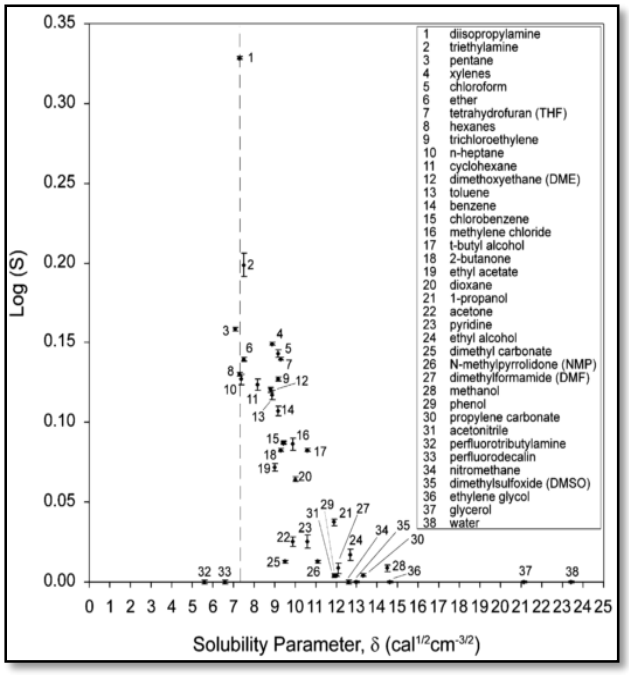

The solvents with solubility parameter same or near to PDMS (δ = 7.3 $cal^{\frac{1}{2}}cm^{\frac{-3}{2}}$) swell PDMS the most [21] [22]. The swelling rate of solvents is shown in Figure 2.2 [23].

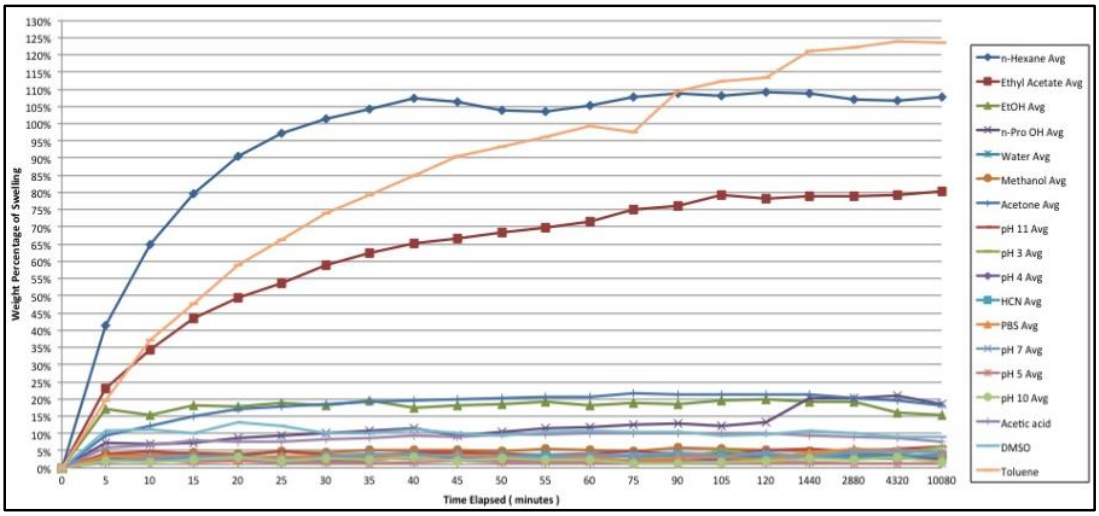

Figure 2.2 Swelling Rate of Solvents in PDMS [23].

2.6 PDMS Swelling Mechanism

PDMS has been widely used in developing applications in microfluidic systems and MEMS [24] [25] but the property of swelling is considered as a negative characteristic in most of these applications. Other applications which have utilized PDMS swelling property is in the bio-replication of adjustable micro-riblets of shark skin to study the drag reduction property of shark skin (shark skin effect) [26] and development of actuators and sensors where swelling of PDMS displaces a feed loop in RFID sensor and hence acts as a mechanical actuator [27].

In order to obtain an estimate of the amount of swelling and the time required to obtain deformation, it is important to understand the swelling mechanism and the transport process of solvents in PDMS. Various transport models have been proposed to explain the complex interactions between the solvent and the membrane material due to the mass transfer of the solvent. When PDMS is placed in a solvent, in general the transportation can be described in the following steps:

1. Adsorption of solvent in the top layer
2. Diffusion of solvent through PDMS
3. Swelling of PDMS

The solvent-polymer interaction is dependent on various factors [28] [29] such as the permeability, viscosity of solvent, surface tension etc. and hence is difficult to capture in one single model. Physical transport models like pore-flow model and chemical transport models like solution-diffusion model have been developed to understand the solvent-polymer interaction [29] but a single model cannot completely describe the behavior. With the dynamics of swelling, the factors governing diffusion through the polymer keep changing and hence the entire transport mechanism never follows a single law throughout the entire process. It is important to note that due to the swelling of the polymer, the diffusion process might depart from Fickian [29].

Swelling of PDMS has been studied experimentally and explained using thermodynamics properties and the elastic deformations caused in the PDMS network. The free-energy due to mixing and elastic deformation have been combined to propose a single model of PDMS swelling. As the solvent diffuses through the PDMS, the cross links in the polymer network start deforming, resulting in elastic deformations and hence in the decrease of swelling ratio with time [30] [31]. In order to quantify swelling of PDMS with various solvents, parameters like solubility, swelling ratio, dipole moment have been reported. Solubility parameter of solvents is one of the major factors which relate to the amount of swelling caused by a given solvent. The fact that solvents with similar solubility parameter as PDMS cause maximum swelling effect in PDMS is established by the Hilderband-Scatchard equation which relates the solubility parameter with the enthalpy

change [21]. Swelling mechanism can thus be explained as the disruption of the cross-linked PDMS network by the excessive solvent diffusing in it which results in elastic deformations and results in volume expansion.

3. PATTERN TRANSFORMATION AND SELF-SEALING EFFECT

In order to fabricate a breathable yet self-sealing fabric, it is important to identify the size range for the initial openings of the pores. This concept of the design i.e. the optimal geometry of the initial pore geometry needed to provide fast self-sealing is discussed in this section.

3.1 Mechanisms

The alteration of the shape and size of periodic polymeric nano- and micro-structures to external stimuli is called pattern transformation [32]. It is mainly due to the fact that at such small scales, the properties are highly sensitive to the details of the polymer structure [33]. Depending upon the external stimuli, the cause of transformation can be mechanical compression [34] [35], solvent swelling [36] [33] and capillary forces [32] . This technique has been used to develop novel devices such as microlens arrays, stretchable electronics [37], memory and logic layouts, phononic and photonic crystals, and surfaces with tunable wetting properties [32].

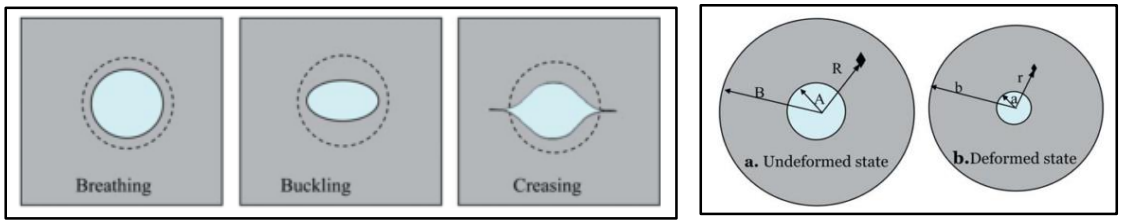

Figure 3.1 Types of Deformation with Increasing Magnitude of Tension and Breathing State in Deformation [38].

The driving force causing the deformation of the nano/micro-pattern is dependent upon the external stimulus. In case of mechanical load, elastic instability is the major cause of

transformations, which are reversible and repeatable. When an external load is applied, the ligaments connecting the holes undergo buckling instability. This results in stresses which when relieved causes pattern transformation [35].

When a liquid-gas interface is present in the hole/void of a periodic polymer structure it can result in capillary tension building up and deformation of the elastomer. There are three principle modes of deformation known as breathing state, buckling, and creasing [38]. The breathing mode occurs when the deformation is driven by internal stresses. This results in change in the size, but not of the shape of the individual features (Figure 3.1). High surface tension liquids can cause deformation of the feature shape and symmetry leading to buckling. In turn, creasing is observed when deformation occurs under constraint. The inner surface remains smooth initially but then creases due to the high tension of the liquid present in the void. The basic difference between these deformations is explained by Figure 3.1. Figure 3.2 illustrates how the increase in the tension inside the hole causes increase in the stress inside the polymer which is then released resulting in deformation due to creasing mode and hence the self-sealing effect.

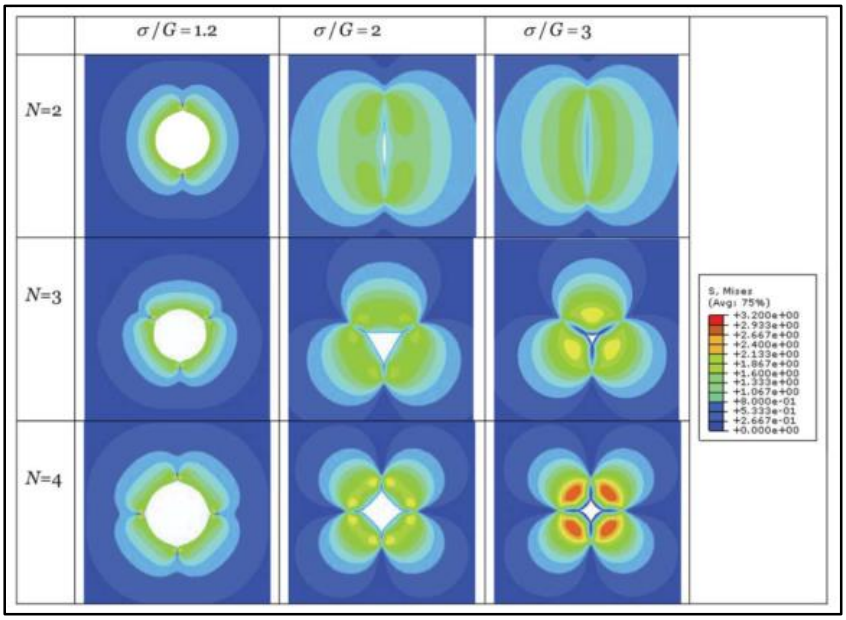

Figure 3.2 Deformation During Creasing for Different Number of Creases (N) for Various Normalized Stress Values (σ/G) [38].

The pattern transformation concept has been used with common polymers such as PDMS and PHEMA. The concept of pattern transformation has been used with of hydrogel poly (2 hydroxyethyl methacrylate) PHEMA which is used in contact lenses and tissue scaffold [32]. Figure 3.3 shows micro patterns formed using PHEMA in undeformed state 'a', swollen breathing state 'b', and deformed shape pattern diamond-like buckling state 'c' after immersion in water. The breathing mode of deformation is observed during the swelling stage. When the water evaporates the hole shrinks as axial compression acts on the swollen wall. This compression force essentially balances the tension created by water-air interface [32]. The relation between capillary pressure σ (hydrostatic tension), surface tension γ_{LV} , contact angle of water at hydrogel interface θ and hole radius r_p is given by [32]:

$$\sigma = \frac{2\gamma_{LV}\cos\theta}{r_p} \tag{2.1}$$

As the hydrogel keeps contracting, the equilibrium meniscus radius r_m decreases because the sharpness of meniscus increases. Thus, the gel keeps shrinking until $r_m = r_p$ and compressive stresses do not increase further [32].

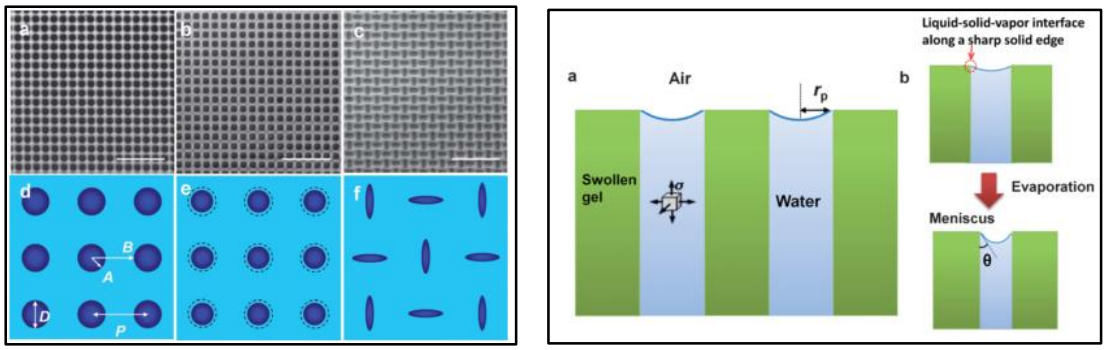

Figure 3.3 PHEMA Pattern Transformation Mechanism [32].

3.2 Micro-Array of Holes-PDMS Hole Pattern Self-Sealing Concept Validation

A PDMS membrane with periodic micro holes has been used to demonstrate pattern transformation due to swelling by several solvents. Previously, the swelling ability of PDMS has been used to develop novel tunable photonics [39] and photonic devices [33]. Here the periodic array of microholes was obtained through dip coating different size woven stainless steel meshes in PDMS. Table 3.1 shows the various available mesh sizes, and the 100M mesh with ~140µm opening and ~115µm wire diameter was selected for making the prototypes.

Table 3.1 Details of Mesh Sizes Available

Sr. No.	Mesh	Mesh size (No. of wires per inch)	Wire Diameter (in inches)	Wire Diameter (in µm)	Opening (in inches)	Opening (in µm)	% opening
1	42 M × 0.0055"	42	0.0055	139.7	0.018	457.2	59
2	60 M × 0.0075"	60	0.0075	190.5	0.009	228.6	31
3	100 M × 0.0045"	100	0.0045	114.3	0.0055	139.7	30
4	200 M × 0.0016"	200	0.0016	40.64	0.0034	86.36	46
5	500 M × 0.0008"	500	0.0008	20.32	0.0012	30.48	36

The dip-coating method was employed to obtain a conformal coating of PDMS on the mesh. Prior to dip coating, the uncured PDMS was diluted with cyclohexane [40] to reduce its viscosity. 1 inch × 1 inch 100M metal mesh samples were cleaned with acetone and dipped for 15 seconds in diluted mixture with 1:10:10 of PDMS curing agent: PDMS base: Cyclohexane by weight ratio. In order to prevent PDMS from blocking the mesh openings, pressurized air at 1.5 psi was blown for 10 seconds on the sample. Next, the samples were cured for 20 minutes at 120°C on the hot plate. After the sample cooled down, the dip-coating and curing process was repeated.

The optimum number of dip-coating and curing cycles that maximizes the amount of deposited PDMS while avoiding blocking of mesh openings was determined iteratively. The process was repeated up to eight times with the same dilution ratio and best results were obtained for 6 dip-coating and curing cycles. The SEM images of the samples are shown in Figure 3.4. In this case the non-uniformity of the hole sizes is advantageous as is allowed for rapid exploration of the hole size evolution after exposure to different solvents.

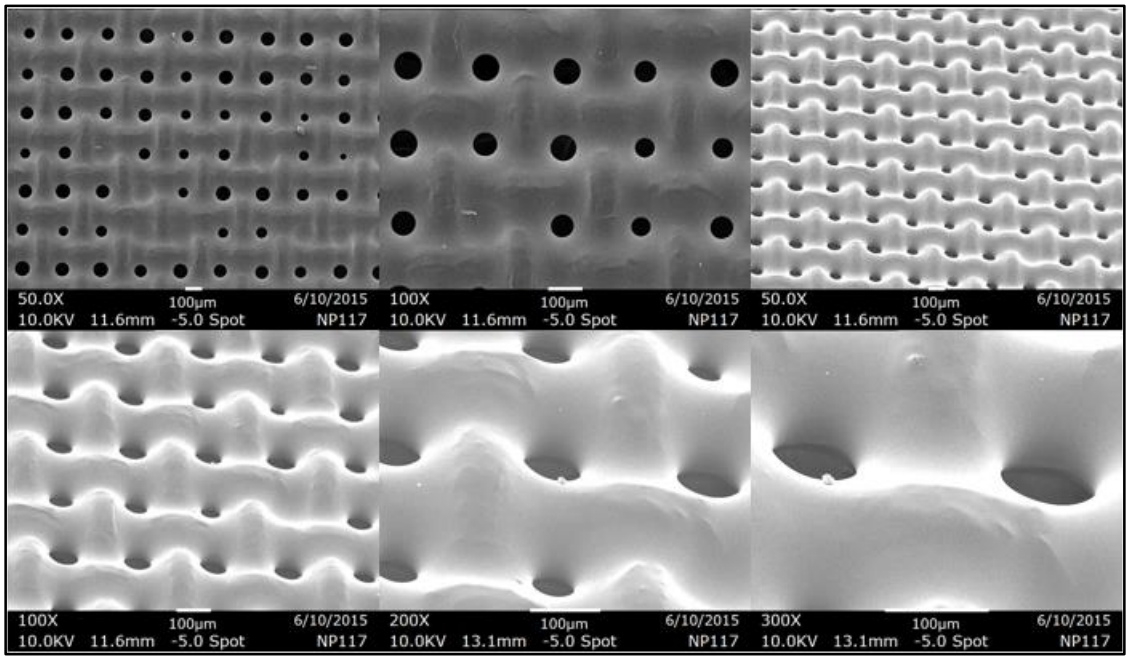

Figure 3.4 SEM Images of 100M Mesh Conformally Coated with PDMS.

The amount of PDMS coated on the mesh after 6 coatings is quantified by measuring the weight of mesh before and after dip coating. ~0.05g of PDMS per 6.25 cm^2 was deposited after 6 dip-coating and curing cycles.

In order to observe the closing of the holes surrounded by PDMS, suitable solvents were selected. The selection of the solvent was based upon the solvent compatibility and swelling characteristics of PDMS as discussed in the previous chapter. As per Table 2.1 [21] and Figure 2.2 [23], three solvents-10cST Silicone Oil, Acetone, and Toluene were selected to conduct the swelling experiments. The PDMS-coated mesh sample was immersed in a petri-dish filled with the solvent. The entire setup was kept under the microscope in order to observe the behavior of swelling and pore-closing process. It was observed that major decrease in the pore diameter occurred only during initial 30 minutes

of soaking. The images in Figure 3.5 illustrate show examples of decrease in the pore diameter for the three solvents used.

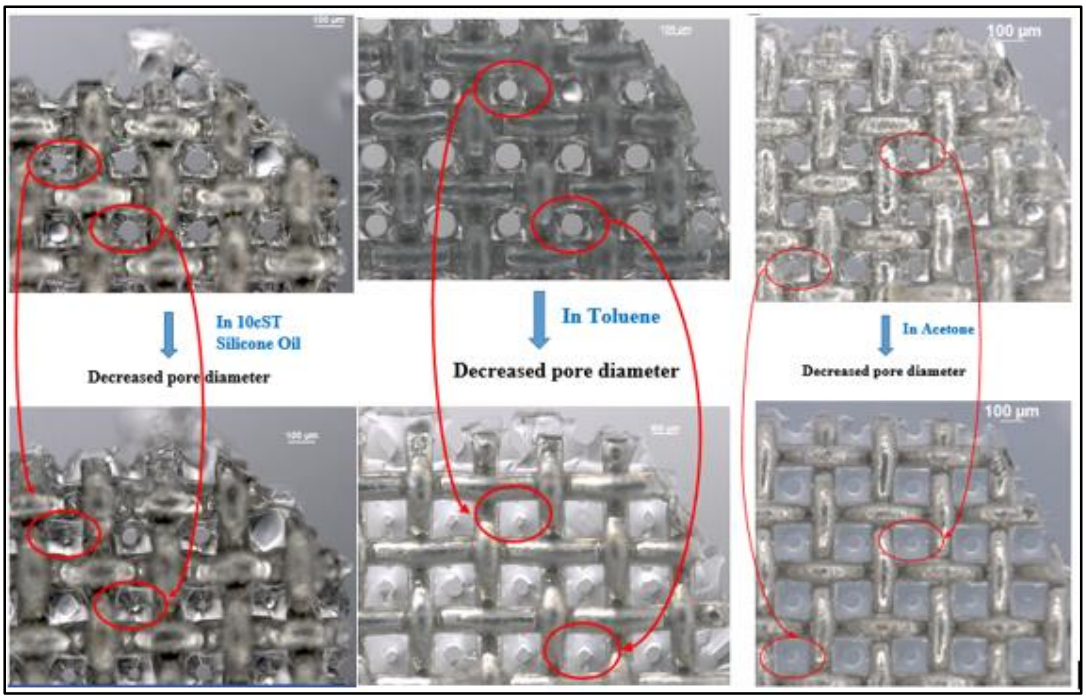

Figure 3.5 Decrease in the Pore Diameter Due to Swelling in Different Solvents.

When the liquid causing swelling evaporates the original shape is recovered in elastic polymes [36] [38] [39]. This mechanism of snapping back to the undeformed shape is observed in the PDMS-coated mesh samples which are dipped in toluene and acetone. Since toluene and acetone evaporate quickly at room conditions, the deformed pores are observed to return to their original size. This behavior was also observed in the case of 10 cSt silicone oil, but after a significantly longer time period.

The variation in the type of deformation pattern was observed depending upon the solvent used. The sample immersed in acetone shows deformation by decrease in the diameter but the circular shape remains intact. Observing this feature, it can be said that

the deformation is breathing type deformation. The deformed samples after immersion in toluene and 10 cSt silicone Oil show deformation by decrease in the size as well the change in shape. The non-retention of circular shape makes this deformation similar to creasing mode deformation. Figure 3.6 illustrates the different modes through which deformation occurs in the swelling experiments.

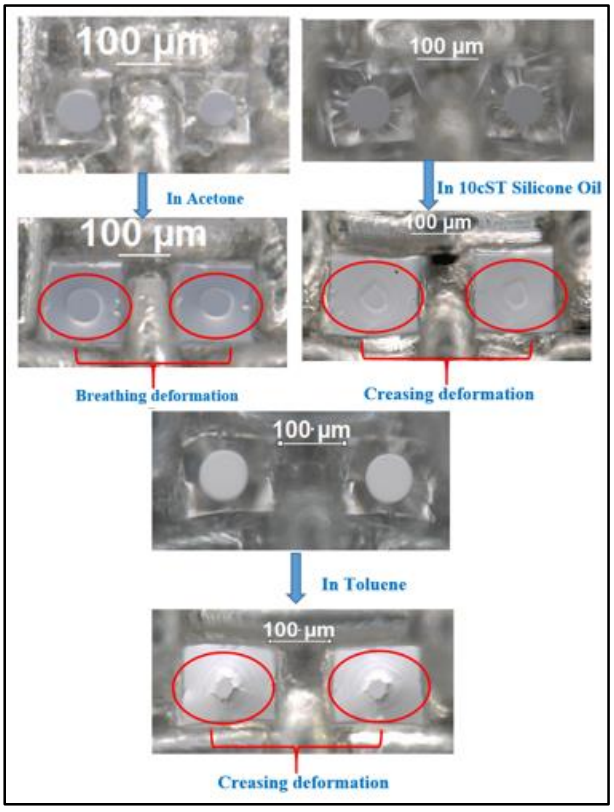

Figure 3.6 Modes of Deformation in PDMS with Different Solvents.

The relation between the diameter of the pore before and after deformation was quantified through image analysis. It was found that the relation is linear with the slope of the straight line dependent upon the solvent responsible for swelling. Results of the image analysis are plotted in Figure 3.7.

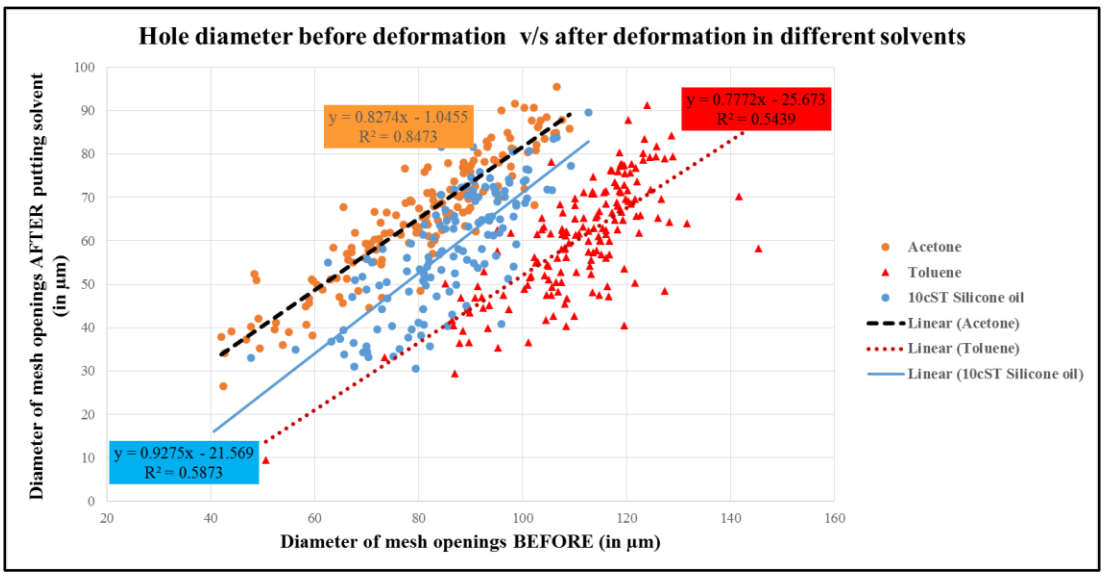

Figure 3.7 Comparative Analysis of Initial and Deformed Pore Diameter in PDMS Coated Mesh After Immersing in Different Solvents.

The linear fits from **Error! Reference source not found.** can be used to obtain an estimate of the range of diameter the pore should initially have in order to obtain complete closing of the pores and hence be used for blocking CWA aerosols. The smaller is the initial diameter, the more efficient is the swelling which means complete closure of the pores can be obtained. Table 3. illustrates the initial diameter required for the three solvents which will result in complete closing of the holes. As previously reported, Toluene has the highest swelling ratio of 1.31 compared to silicone oil (1.08) and acetone (1.06) [21] [22] and the experimental results from Figure 3.7 are in agreement with these swelling ratios as toluene results in complete closing of the largest hole diameter of ~33 µµm compared to silicone oil and acetone.

Table 3.2 Initial Diameter of Hole to Achieve Complete Hole Closing Based on Linear Equation Fit of Experimental Results

Solvent	Linear fit equation y = ax + b	Initial diameter of hole to achieve complete hole closing [in μm] (y = 0 $=> x = \frac{b}{a}$)	Swelling Ratio
Toluene	$y = 0.7772x - 25.673$	33.03±8.19	1.31 [21]
10cST Silicone Oil	$y = 0.9275x - 21.569$	23.25±6.46	1.23
Acetone	$y = 0.8274x - 1.0455$	1.26±2.74	1.06 [21]

The small size of original pores needed to produce a sealed barrier for swelling ratio of 1.06 to 1.31 imply that polymers with significantly higher swelling ratio are needed for more open and breathable fabrics. The use of such superabsorbing polymers for our design is discussed in next Chapters.

4. SUPERABSORBENT POLYMERS (SAPs)

The results from Chapter 3 showed that very high swelling ratios are necessary in order to have sealable pores that have "open state" size higher than a few micrometers. In order to explore use of higher swelling material-liquid pairs, several new mesh prototypes were fabricated using water superabsorbent polymers (SAPs). This chapter provides overview of SAP characteristics, and droplet interactions with water SAP films applied from liquid solution as well as PDMS-SAP composites.

4.1 SAP Characteristics and Applications

SAPs are a special class of hydrogels that due to their hydrophilic network can absorb large amount of water without getting dissolved (up to 300 times their own weight) [41]. Their special feature of absorbing huge amount of water and expanding is attributed to their structure. For example, some water SAPs consist of long chains of linear polymers of cross-linked Poly (Acrylic Acid) chains that are sparsely interconnected. When placed in water, they absorb water due to osmotic pressure. Absorption of the liquid leads to expansion in the volume as the water enters the space between the long polymer chains and the cross links [42].

SAPs are commonly used in hygiene products and in agriculture industry for controlled release of pesticides in soil as well as increasing the capability of soil to retain moisture and nutrients [43] [44] [45]. SAPs are also used in other areas such as fire-fighting, food packaging, and electrical cable isolation [46] [43]. For the latter application, water swellable coatings have been invented using dispersion of SAP particles in liquid plastisol. Upon exposure to water, this coating swells and fills the gaps in the cable rendering the

cable watertight and hence protects the fiber optic component [47]. SAPs as additives are also used for self-sealing of cracks in concrete and for strengthening of concrete [48] [43]. The property of SAPs to undergo large changes in the swelling ratio makes their application in bio-separation possible and hence they are also used to separate proteins [43]. The swelling property of SAP has also been utilized to fabricate reactive seals for body suits which when come in contact with water swell the polymer and hence result in sealing. The seal made from SAP can be placed in different parts of the body suit like neck, wrist, ankle and other required places such that the body suit is comfortable to wear at all times and applies required sealing pressure only when exposed to water. This sealing action takes place instantly within 10 to 15 seconds due to the high swelling rate of the SAP [49] .

For the exploratory proof-of-concept experiments conducted in this thesis, water responsive SAPs were utilized. For the actual fabrics, special SAP polymers that are responsive to a wide range of organic liquids, but not water, will be synthesized.

4.2 Characterization of Liquid SAP Films-Effect of Thickness

In order to systematically explore water droplet behavior on SAP, liquid SAP (LiquiBlock™ DGS, Emerging Technologies) was used to cast SAP films. The liquid SAP is diluted with water (1:5 by weight SAP to DI water), manually stirred, and degassed. The diluted SAP is then poured into an aluminum petri dish and cured at 120°C for 6 hours. 100 µm and 300 µm thick SAP films were fabricated to conduct sessile droplet experiments.

1 µL DI water droplets were placed on two samples with the varying thickness. The top view and side view of the drop absorption process are as shown in Figure 4.1. It can be seen in the top view that the polymer deforms more for the 100 µm thick film than for 300 µm film. In the case of 300 µm thick film, no irregularities are visible from the top view. It is clear from the side view that the water droplet laterally diffuses within both the films. The self-deformation mechanism is evident from the top view of 100 µm thick film, which is desirable for the self-sealing feature of protective gear. In the 300 µm thick film, the top view shows the droplet only getting diffused across the thickness of material and increase in the area of drop can be seen in Figure 4.1(b).

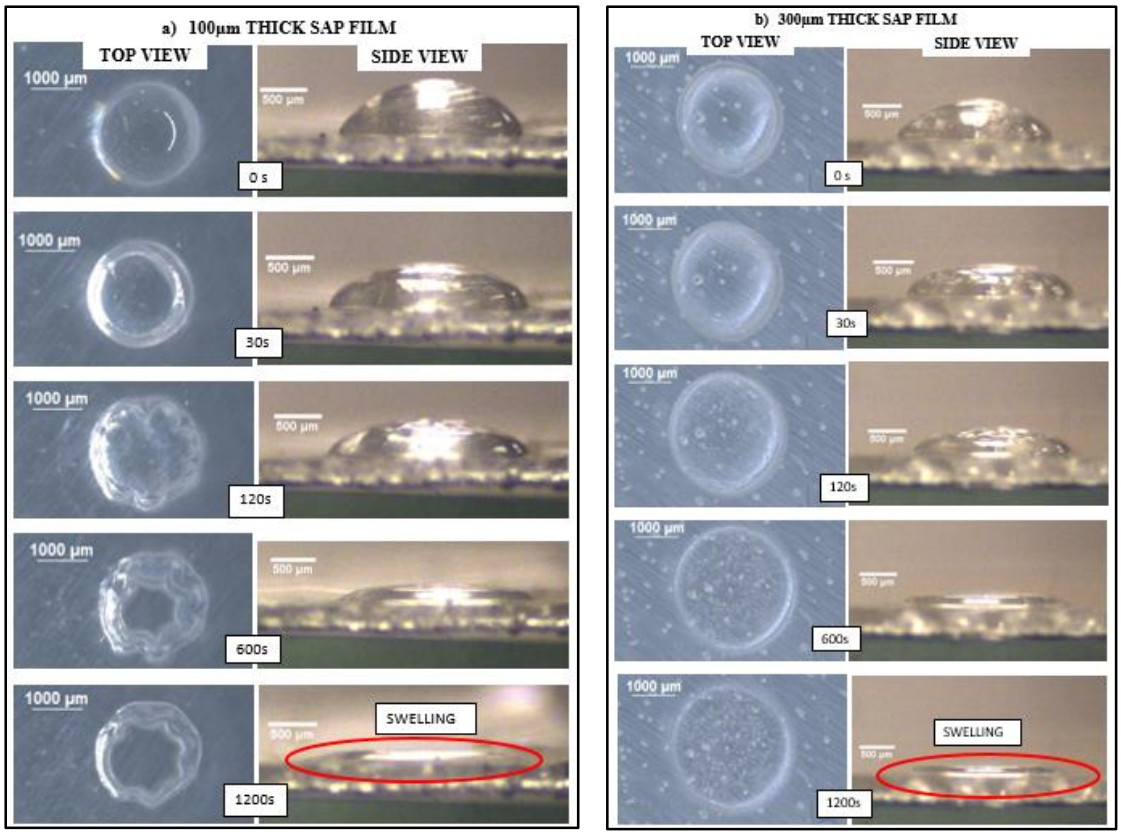

Figure 4.1 Behavior of Sessile Water Droplet on the Liquid SAP Film.

Unfortunately, the swollen liquid SAP films were found to be difficult to handle and work with, consequently further experiments described in following Chapters were conducted using SAP microparticle and elastomer composites.

5. SAP MICROPARTICLES AND ELASTOMER COMPOSITES

The use of SAP particles in PDMS has been previously reported to increase the inorganic salts permeability through PDMS due to the areas swollen by water absorbed SAP particles. SAP as additives in the PDMS matrix results in increase of water penetration inside when a threshold of swollen SAP is present which is beneficial in applications like durable wound adhesives [50]. This chapter describes use of SAP microparticle-PDMS composite as a highly responsive and stretchable swelling coating.

5.1 Characterization of Used SAP (Sodium Polyacrylate) Microparticles and Composite Fabrication

Sodium Polyacrylate is one of the most widely used SAPs and its swelling property is attributed to the sodium ions present in polymer network. When exposed to water, the sodium ions in the polymer network have a tendency to dissociate from the network and move into the liquid. Consequently, replacement of the sodium in the polymer network by hydrogen in the water molecules results in swelling of the SAP [51] [52] [53]. The degree of swelling of sodium polyacrylate particles is dependent on purity of the surrounding water, as the presence of salts and minerals decreases the swelling ratio [51] [54] [55]. Thus in order to see the maximum swelling in the samples, DI water is used in all experiments.

Size distribution of the SAP particles is an important factor to obtain homogenous dispersion of particles in the PDMS matrix during sample preparation. Sodium polyacrylate dust purchased from AquaSorb was used and has been categorized as finest (25 µm), fine (46 µm) and coarse particles (85 µm) by grinding them using Mortar and

Pestle and sieving them through various size meshes. Figure 5.1 shows the particle size distribution of the three powders obtained from analysis of SEM images.

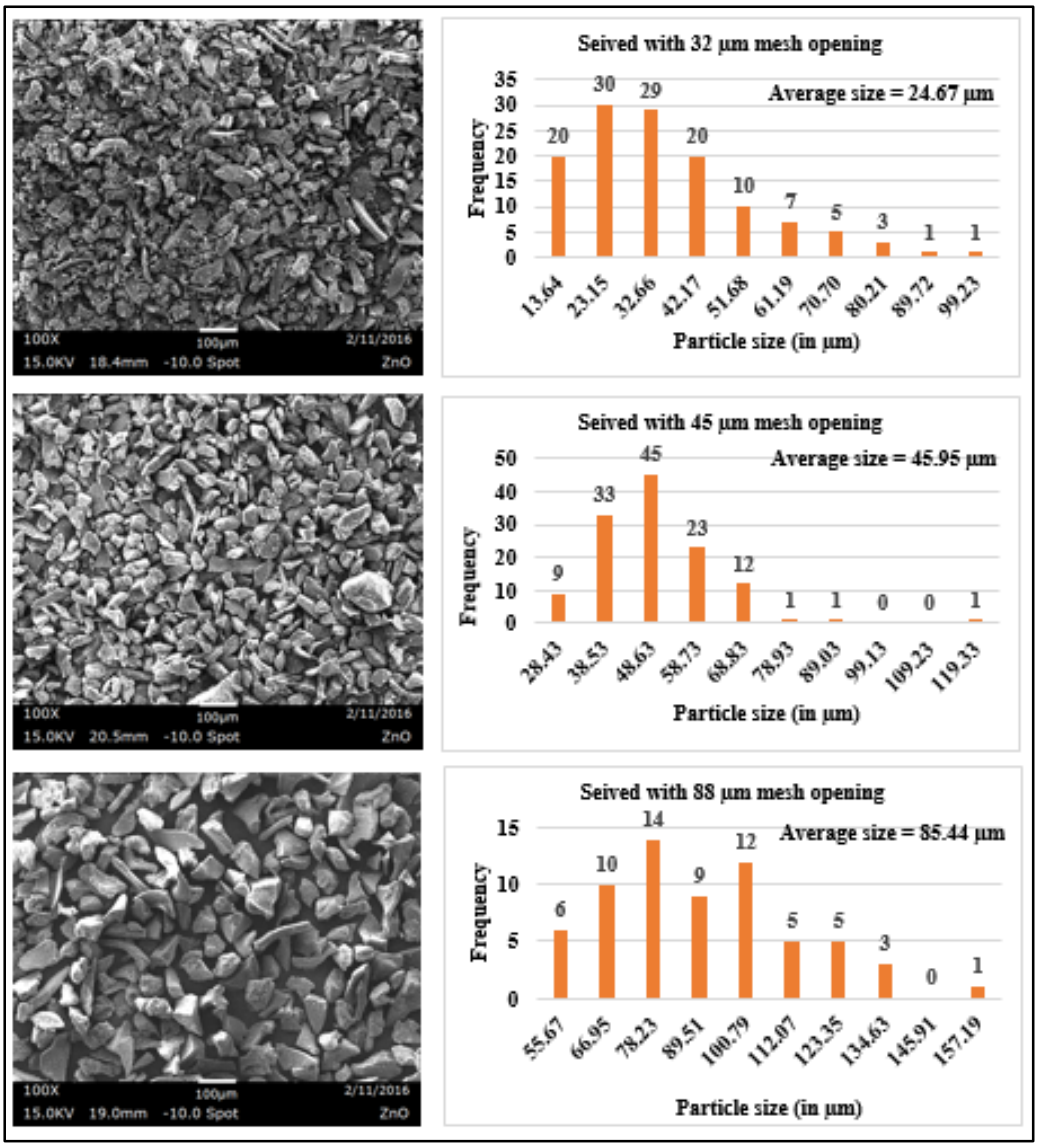

Figure 5.1 SAP Particle Size Distribution of a) Finest, b) Fine and c) Coarse SAP Particles.

Films of two different thicknesses were made using the SAP powder (46 µm) and PDMS mixed in 1:2 ratio by weight. The mixing is done for 2 minutes using high speed stirrer at 1500 rpm and the curing agent is added at the end of 1 minute in the SAP-PDMS

matrix to prevent the cross-linking of PDMS and curing agent due to heating up of the mixture while high speed stirring. This homogeneous mixture is then spin-coated on Teflon at 1500 rpm for 10 seconds and cured at 120°C for 20 minutes to obtain PDMS-SAP thin film of 200µm thickness. In order to obtain a thicker slab, the PDMS-SAP mixture is poured in a 3-D printed mold to obtain 3500 µm thick slabs.

5.2 Behavior of Sessile Water Drops on the Composite Films

The behavior of 1µL sessile droplet is observed on only SAP particles film (46 µm in size) and on PDMS-SAP films with thickness of 200 µm and 5000 µm. In order to characterize the swelling behavior of the sodium polyacrylate SAP particles, control experiment was conducted with only SAP particles spread on the top surface of a double sided tape. The images in Figure 5.2 show absorption of a 1 µL DI water drop dyed using methylene blue solution (diameter of 1500 µm) on top of the films. The swelling of SAP particles occurs in the first 5 seconds after placing the droplet and desorption from the swollen SAP particles starts after a minute and within 10 minutes the SAP particles de-swells completely.

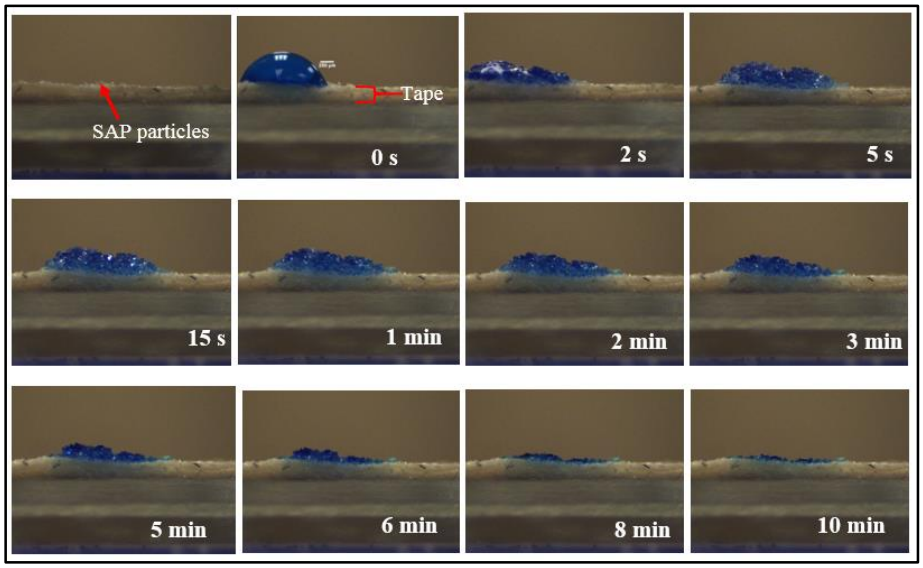

Figure 5.2 Behavior of Water Droplet on Only SAP Particles.

Figure 5.3 a) shows the behavior of 1 µL dyed (using methylene blue solution) DI water droplet (diameter of 1500 µm) on 200 µm and 5000 µm thick PDMS-SAP composite films. Localized deformation in thin film (200 µm) becomes evident by the formation of gel 2-3 minutes after the water droplet is placed on the film. Due to the localized swelling caused, internal stresses develop in the film. This causes bending which becomes evident after 15 minutes as highlighted in the side view of Figure 5.3. The location where the water drop is placed is converted to SAP swelled region after 3 minutes after which multiple creases keep appearing where initially water droplet was placed. These multiple creases are the boundaries of the individual swollen SAP particles. The swollen SAP particles start de-swelling after 20 minutes as the water starts evaporating. After one hour complete de-swelling takes place with no traces of any swollen SAP on the film. The de-swelling of the SAP particles can be observed in the top view and as shown in Figure 5.3 a), a patch of SAP particles is visible at the location the drop was placed.

Figure 5.3 Sessile Water Droplet on a) 200 µm b) 5000 µm Thick PDMS-SAP Film.

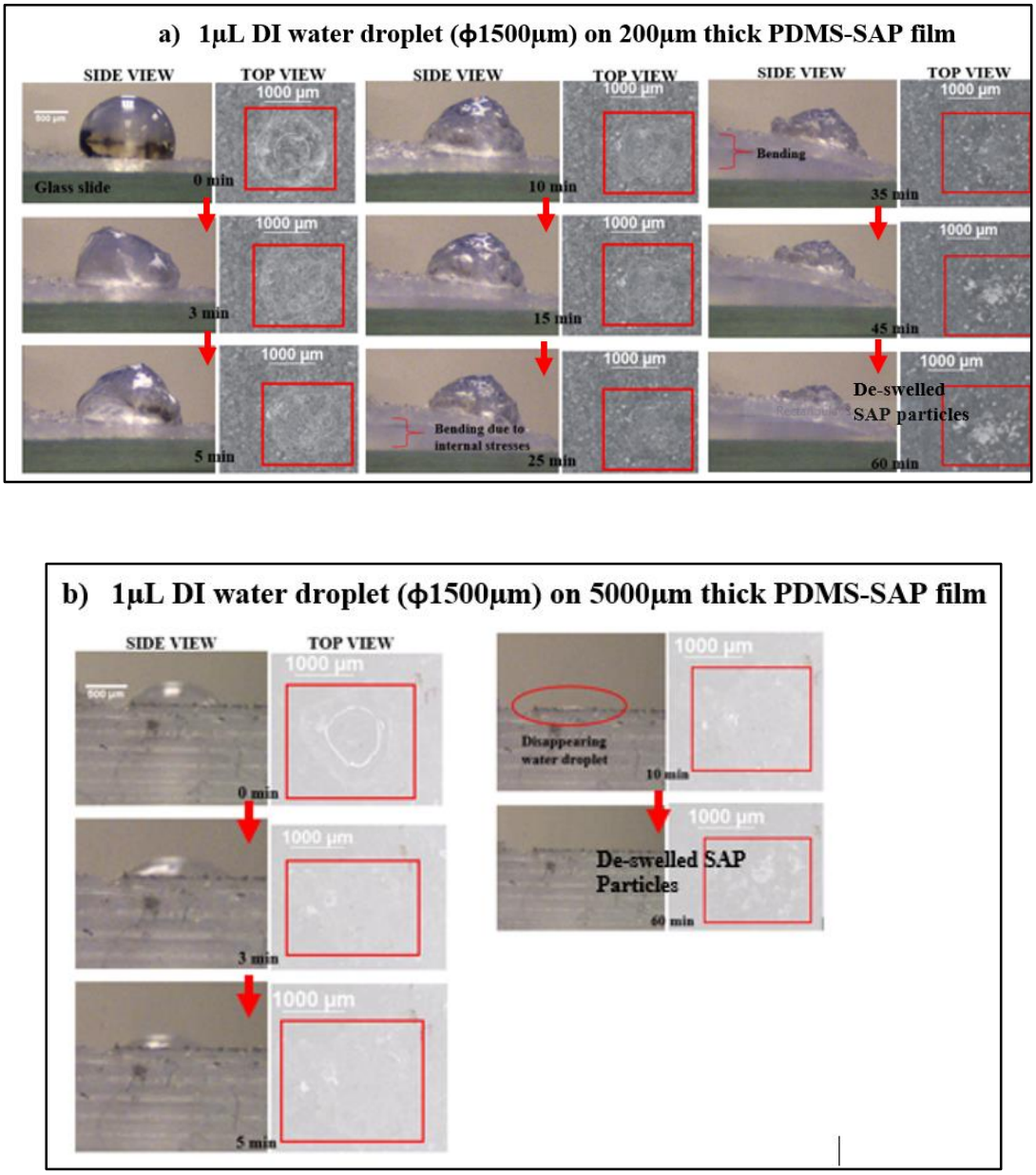

Images in Figure 5.3 b show behavior of the 1 µL DI water droplet placed on 5000 µm thick film. In this case no visible local deformation is observed in the side view as was seen in the case of thin composite film. As in the case of thin film, the swollen SAP particles start de-swelling after 20 minutes and after one hour de-swelling is completed.

Same experiments were conducted for 10 µL sessile DI water droplet (diameter of 2500 µm) on both the films and the similar, albeit slower, localized deformation, swelling and de-swelling processes were observed.

6. DEVELOPMENT OF MICRO-FLUIDIC NETWORK: TOWARDS RAPIDLY SELF-SEALING CONFORMAL COATING USING SAP PARTICLES IN HYDROPHOBIC MATERIAL

The characterization of SAP particles and PDMS matrix embedded with SAP particles has been discussed in the previous chapter and it can be said that the inclusion of SAP particles in PDMS matrix results in an interesting blend of properties of hydrophobic and super-absorbing surfaces. This chapter focuses on the method to obtain a breathable, self-sealing mesh design which incorporates additional features to the concept validation design proposed previously using PDMS. This design has features of super absorption and hydrophobicity in addition to pattern transformation and swelling to achieve efficient sealing.

6.1 Fabrication of SAP-PDMS Composite Covered Meshes

The design requirement of pattern transformation i.e. periodic array of microholes was obtained through the process of dip coating different size stainless steel meshes. Conformal coatings on the meshes were obtained by ensuring a homogeneous SAP–PDMS mixture, adjusting viscosity of the solution using solvents, and changing the dip coating and curing cycle number. 60M mesh (~230 µm opening, ~192 µm wire diameter), 100M mesh (~140 µm opening, ~115 µm wire diameter) and 42M mesh (~458 µm opening, ~140 µm wire diameter) were coated with the finest (25 µm), fine (46 µm), and coarse (85 µm) Sodium Polyacrylate particles. In order to obtain a periodic pattern of open array of holes, the viscosity of the PDMS-SAP mixture was lowered using cyclohexane.

1 inch × 1 inch 100M metal mesh samples cleaned with acetone were dipped for 15 s in PDMS-SAP-cyclohexane, 1:2:3 by weight (PDMS:SAP:Cyclohexane). In order to obtain a homogeneous dispersion of SAP particles in PDMS, initially only half of the total amount of cyclohexane is put and the mixture is stirred using a mechanical high speed stirrer at 1500 rpm for 5 minutes. After 3 minutes of stirring, PDMS curing agent and remaining amount of cyclohexane was added and stirred for 2 minutes. This intermittent mixing-stirring approach was adopted to prevent the PDMS from cross-linking due to temperature rise due to stirring and to prevent the entire cyclohexane from evaporating. In order to prevent PDMS-SAP from blocking the mesh openings, pressurized air at 1.5 psi is blown for 10 seconds on the sample after which they were cured for 60 minutes at 150°C on the hot plate. SEM images of representative samples are shown in Figure 6.1. The conformal coating of the mesh with PDMS-SAP and opening of the pores is evident from the SEM images. The SAP particles are mostly embedded in PDMS and firmly attached to the metal mesh.

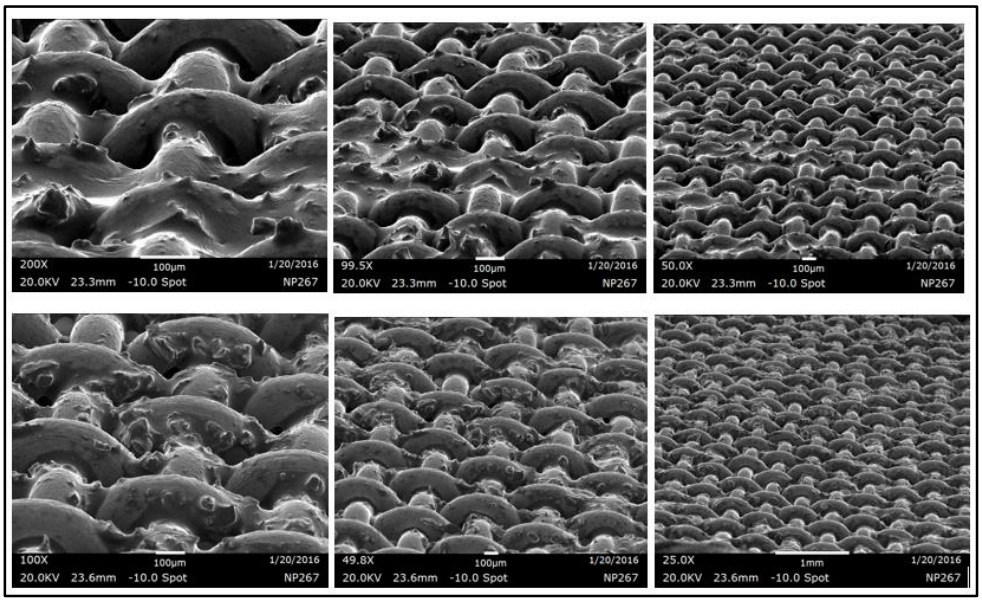

Figure 6.1 SEM Images of Mesh Coated with PDMS-SAP Matrix.

To quantify the amount of PDMS-SAP matrix covering the mesh, weight of the mesh before and after coating is measured and ~0.01g of PDMS-SAP matrix is coated on the 60M mesh, ~0.005g on 100M mesh and ~0.007g on 42M mesh for the PDMS:SAP: Cyclohexane ratio 1:2:3 by weight. The difference in the amount of coating is due to the wire diameter available for the coating, number of dip-coating cycles and upon the dilution ratio. The best results were obtained for the ratio of PDMS: SAP: Cyclohexane as 1:2:3 by weight and single dip-coating.

6.2 Sessile Drop Behavior on the Composite Covered Meshes

The behavior of 1µL sessile water droplet is observed on three different size meshes coated with PDMS-SAP matrix. Figure 6.2 shows behavior of the drop placed on 100M mesh.

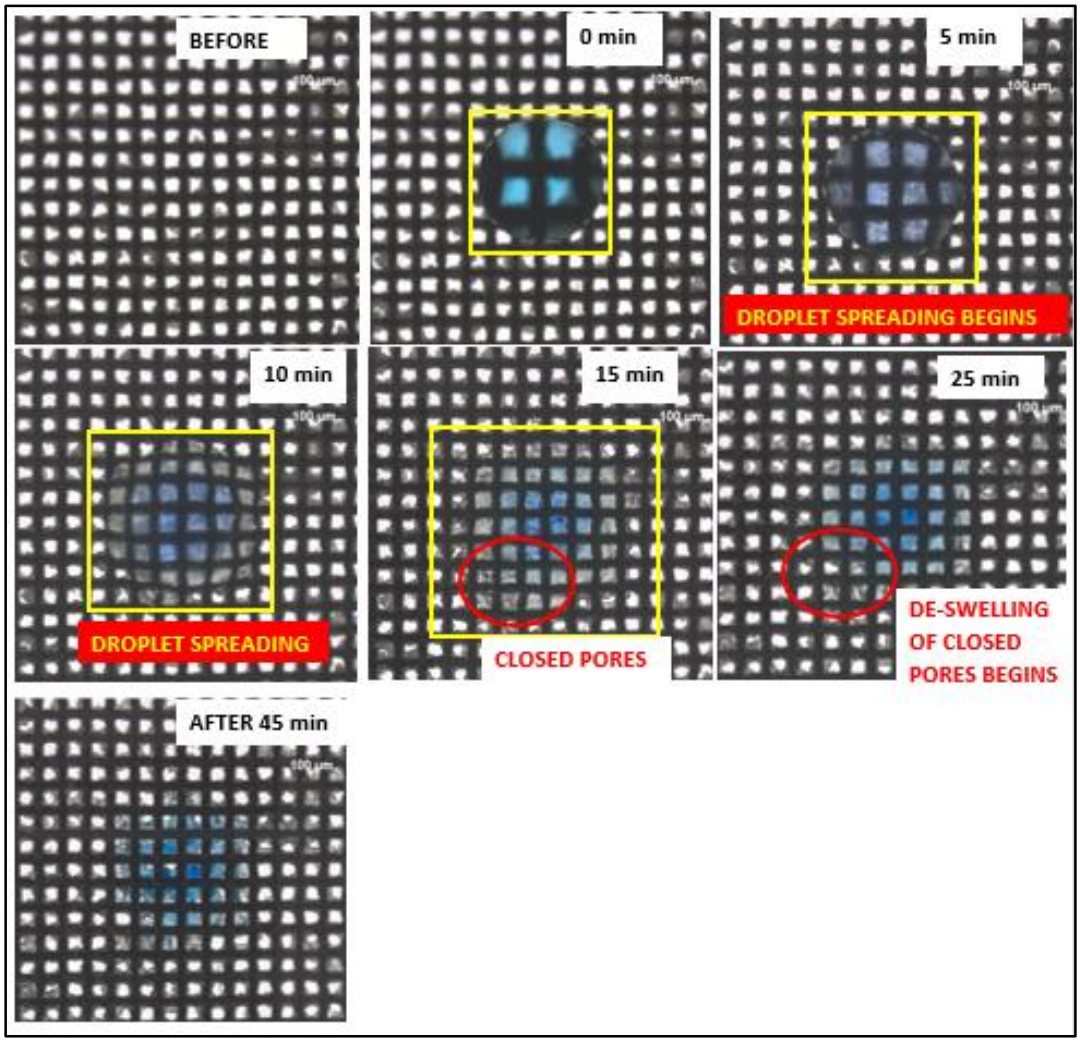

Figure 6.2 Stages of Sessile Droplet on PDMS-SAP Coated 100M Mesh.

As soon as the droplet is placed on the mesh, a change in the transparency of the drop can be observed. This indicates that the SAP particles under the droplet start swelling due to the diffusion of water. Thus diffusion stage begins as soon as the droplet is placed on the mesh. As indicated in Figure 6.2, spreading of the droplet begins 5 minutes after it is placed on the mesh. The processes of diffusion, swelling and spreading co-exist for the first 15 minutes. After 25 minutes it is observed that the closed pores start to open as the swollen SAP particles begin to deswell due to evaporation of water. Figure 6.3 illustrates

the various stages of a sessile droplet on 60M PDMS-SAP coated mesh from an angle which explicitly shows the transition stages of water droplet from liquid to a gel due to SAP swelling.

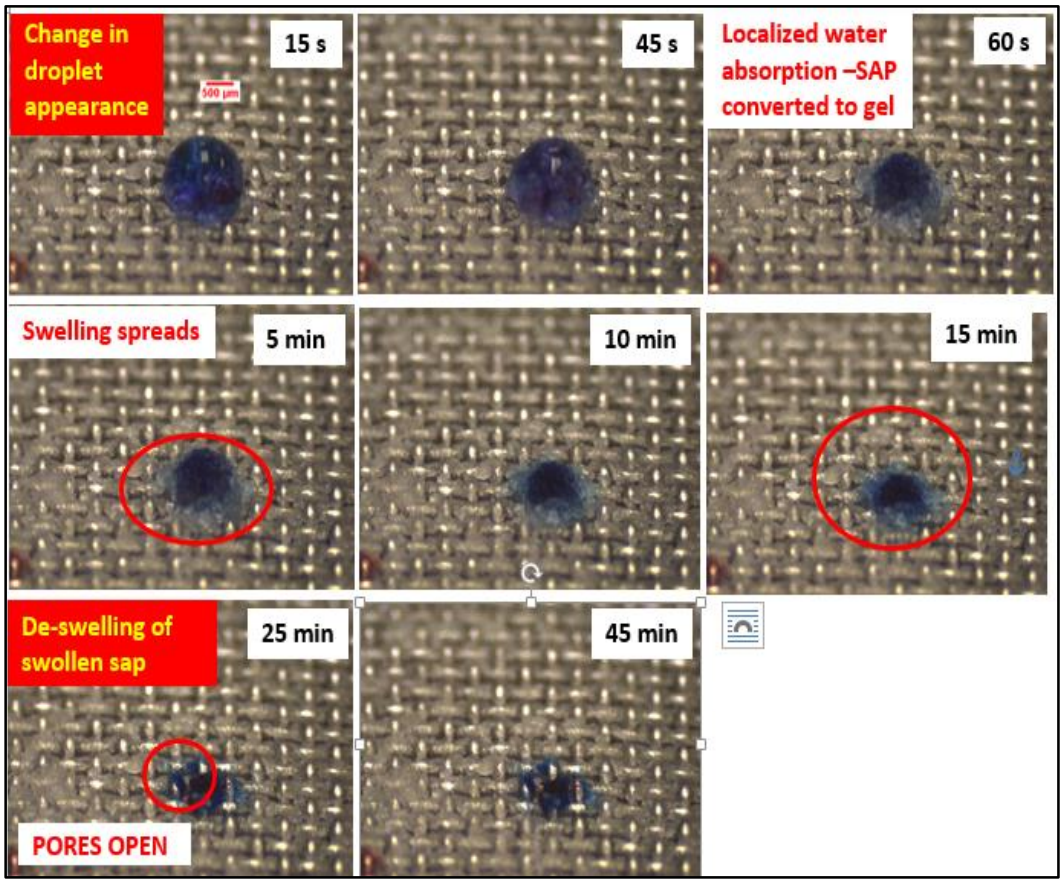

Figure 6.3 Stages of Sessile Droplet on PDMS-SAP Coated 60M Mesh Viewed From an Angle.

Similar experiments were conducted for the other two meshes for all the sizes of the SAP particles. The effect of mesh and particle size is explained in the following section.

Impinging Droplet Behavior on the Composite Covered Meshes

A 10µL droplet from a height of 220mm was impinged on 100M mesh coated with PDMS-SAP matrix and the droplet behaviour was recorded as shown in Figure 6.4.

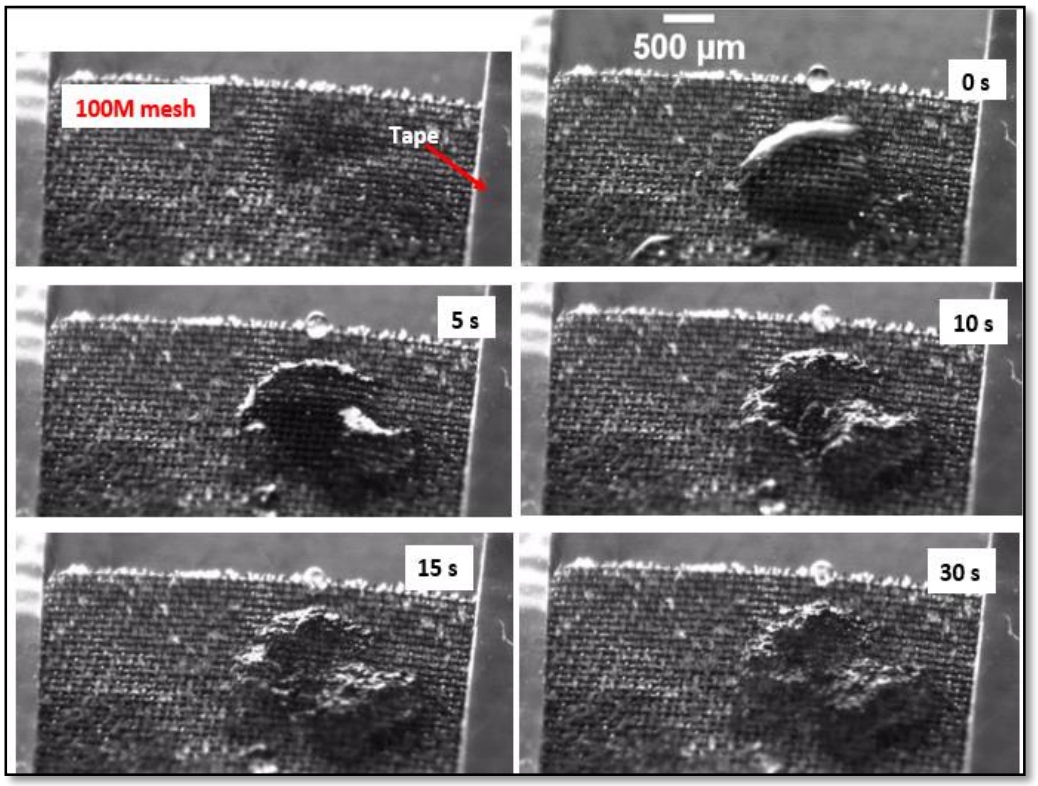

Figure 6.4 Single Drop Impingement on PDMS-SAP Coated 100M Mesh.

As against the sessile droplet, the blockage of pores due to the conversion of droplet to gel was observed rapidly within 10s of impingement. This increase in rate can be attributed to the velocity of the impinging droplet which increases the penetration of water in the PDMS-SAP matrix.

6.4 Effect of Mesh Spacing and Size of SAP Micro Particles on Sealing Speed

The droplet experiments were conducted for 60M (~230 µm opening, ~192 µm wire diameter), 100M (~140 µm opening, ~115 µm wire diameter), and 42M (~458 µm opening, ~140 µm wire diameter) mesh sizes with three different size of SAP particles (finest 25 µm, fine 46 µm and coarse particles 85 µm). The sealing of mesh openings was never observed in 42M mesh due to its large opening size of ~458 µm. Successful closing was observed for both 60M and 100M meshes for all the three particle sizes though the rate of closing is different and is quantified by permeation experiments explained in detail in the last chapter.

Three different size of SAP particles (finest 25 µm, fine 46 µm and coarse particles 85 µm) were used to fabricate samples on three different mesh sizes. Sessile droplet experiments were conducted for the three SAP particle sizes and an interesting observation is made: the sessile droplet placed on the sample caused not only localized swelling but also deformations all across the sample. For example, Figure 6.5 illustrates closing of 60M mesh coated with finest SAP particles (25 µm). This implies formation of a micro-fluidic network in samples made of the fine sized particles.

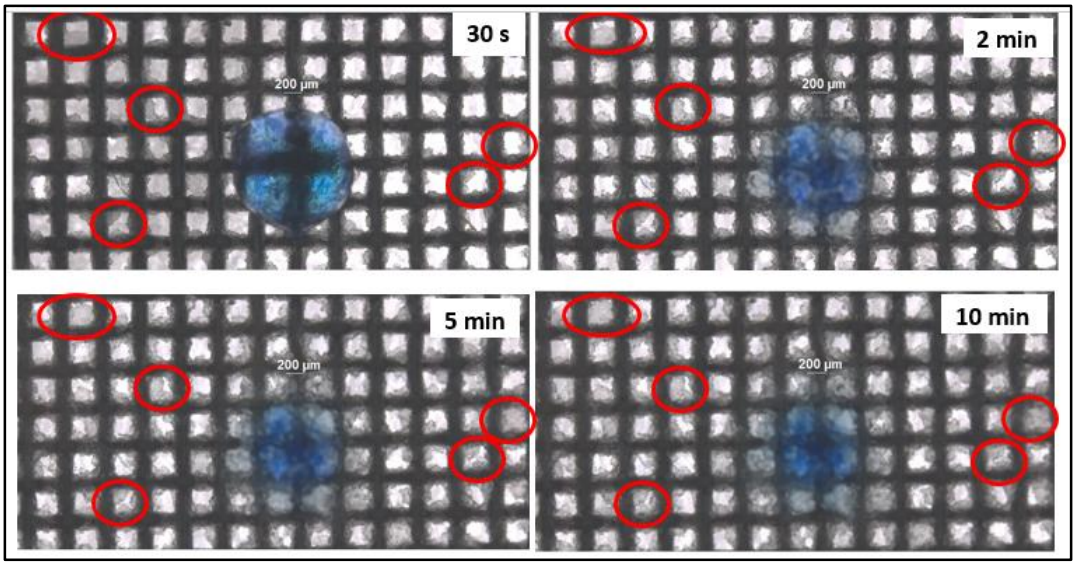

Figure 6.5 Closing of Mesh Openings far Away From the Location of Droplet Due to Micro-Fluidic Network Formed by Fine Micro SAP Particles Homogeneously Dispersed in PDMS.

This observation implies that the fine sized SAP particles form an internal micro-fluidic network that enhances the transport of liquid all across the coated mesh. This enhances the transport mechanism and hence the response time. The "micro-fluidic network" feature of this design makes it a very efficient and effective one as each and every drop of liquid which impinges the surface activates the entire structure and initiates the self-sealing mechanism. This feature is not observed for large particle size (85 µm) and hence the smaller the particle size the better is the transport mechanism.

6.5 Optimal Design for Rapid Self-Sealing Fabrics

On the basis of the mesh opening size, particles size and the sessile droplet experiments, 42M mesh (~458 µm opening, ~140 µm wire diameter) and coating with coarse particles 85 µm are eliminated. 60M (~230 µm opening, ~192 µm wire diameter) and 100M (~140

µm opening, ~115 µm wire diameter) mesh coated with matrix of PDMS and finest SAP particles 25 µm are identified as the optimal geometry on the basis of the micro-fluidic network formation by the finest particles accelerating the transport phenomenon and as per the closing of mesh openings observed in both 60M (~230 µm opening, ~192 µm wire diameter) and 100M (~140 µm opening, ~115 µm wire diameter) meshes.

6.6 Multi-Physics Model of Self-Sealing Coatings

The dynamics of how the diffusion of liquid impacts the mechanical properties of the elastomer is observed experimentally in the form of swelling of the solid. In order to develop a predictive model of the design for different solvents having different swelling ratio, Finite Element Model (FEM) is to be developed. From the experimental observations it can be concluded that the self-sealing mechanism is an integrated model of transport phenomenon (essentially diffusion), swelling and structural mechanics [56]. The case of diffusive transport mechanism is coupled with the structural mechanics of polymer when the polymer is exposed to liquid at the top. Linear elastic properties of the polymer are considered and swelling is modeled using the concentration dependent strain term in COMSOL. Figure 6.6 illustrates the chemo-mechanical process of pore-closing pheomenon obtained using simple diffusion-swelling module .

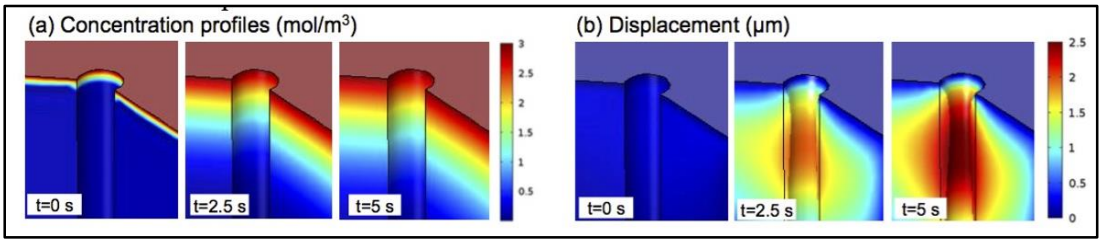

Figure 6.6 COMSOL Simulations When Top Surface is Exposed to Liquid a) Concentration Profile b) Displacement After Exposure.

The transport physics interface is integrated with solid mechanics interface using the hygroscopic swelling 'Multiphysics' module in COMSOL 5.2. Diffusion coefficient is assumed to be constant and the moisture concentration is calculated from the transport of diluted species module using equation 6.1 [57] where *c* is the concentration inside the solid in mol/m^3 and *D* is the Diffusion coefficient in m^2/s.

$$\frac{\partial c}{\partial t} = \nabla.(D\nabla c) \tag{6.1}$$

The calculated concentration is the input to the coupled interface of hygroscopic module and it calculates the inelastic strain ϵ_{hs} developed due to swelling using equation 6.2 [57]. The coefficient of hygroscopic swelling β_h (m^3/kg) is specified in the material properties, M_m is the molar mass (kg/mol) and the mositure concentration c_{mo}(mol/m^3) and strain reference concentration $c_{mo,ref}$ (mol/m^3) are specificed in the model inputs.

$$\epsilon_{hs} = \beta_h M_m\left(c_{mo} - c_{mo,ref}\right) \tag{6.2}$$

This strain is then used by the Solid Mechanics module to find the displacement using the equations 6.3 [57] where ρ (kg/m^3) is the density of the material , u (m) is the displacement and S the elastic compliance tensor [58] which takes into account the strain computed by the hygroscopic swelling module.

$$\rho\frac{\partial^2 u}{\partial t^2} = \nabla.S \tag{6.3}$$

The model can be verified by matching the experimental results with the test case simulations. Once the test case is validated, it can be used for parameteric study by inputting solvents with different swelling ratios. This will help in predicting and comparing the rate of closing and efficiency of the design for different solvents.

7. EFFICIENCY OF SELF-SEALED BARRIER AGAINST AEROSOL SPRAY

In order to measure the effectiveness and efficiency of the barrier formed by the swollen SAP particles, aerosol permeability experiments were conducted by measuring the number of droplets penetrating the samples when exposed to water aerosol spray. These permeation tests were performed on the 60M (~230 µm opening, ~192 µm wire diameter) and 100M (~140 µm opening, ~115 µm wire diameter) meshes coated with matrix of PDMS and finest SAP particles 25 µm as they were identified as the optimal geometry in the previous chapter.

7.1 Setup for Aerosol Permeation Experiments

The experimental setup consists of a wooden stand on which two clamps are fixed such that the mesh samples can be placed between them. The mesh placed is not fixed permanently on the clamp and can be easily lifted and replaced time and again. A glass slide covered with tape is fixed on the wooden clamp right behind the mesh, which will capture the number of droplets penetrating the mesh. Figure 7.1 illustrates the setup used for the experiments. The mesh is not fixed permanently on the clamps because ease of handling the mesh is required in the experiment as after every spray the mesh is removed to capture the number of droplets penetrating the SAP barrier and reaching the taped surface of glass slide. The distance between the mesh sample and glass slide is 3 mm. This distance is kept by taking into consideration the severe case where the protective gear is 3mm away from the human skin. The atomizer used for spraying dyed (using methylene blue solution) DI water is placed 250mm away from the mesh sample. The camera is mounted on the stand and positioned in such a way that it captures the region where the

aerosol strikes the sample. The position of the camera remains fixed throughout the experiment to capture the appropriate area on the mesh and the glass slide.

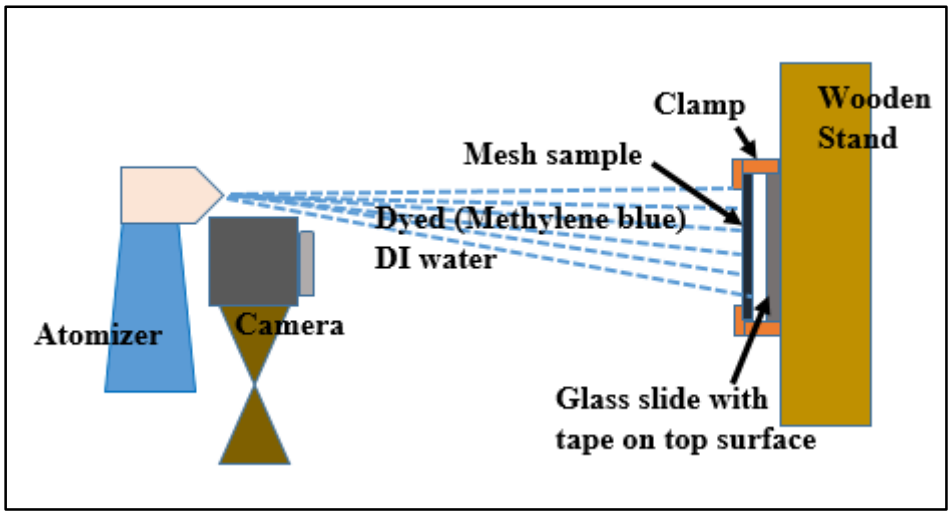

Figure 7.1 Permeation Experimental Setup.

7.2 Aerosol Permeation Results

The 60M (~230µm opening, ~192µm wire diameter) and 100M (~140µm opening, ~115µm wire diameter) meshes coated with matrix of PDMS and finest SAP particles (25 µm) were both subjected to the aerosol spray. Images of the mesh and droplets reaching the glass slide were taken immediately after every spray. Figure 7.2 illustrates the results obtained for both the mesh sizes.

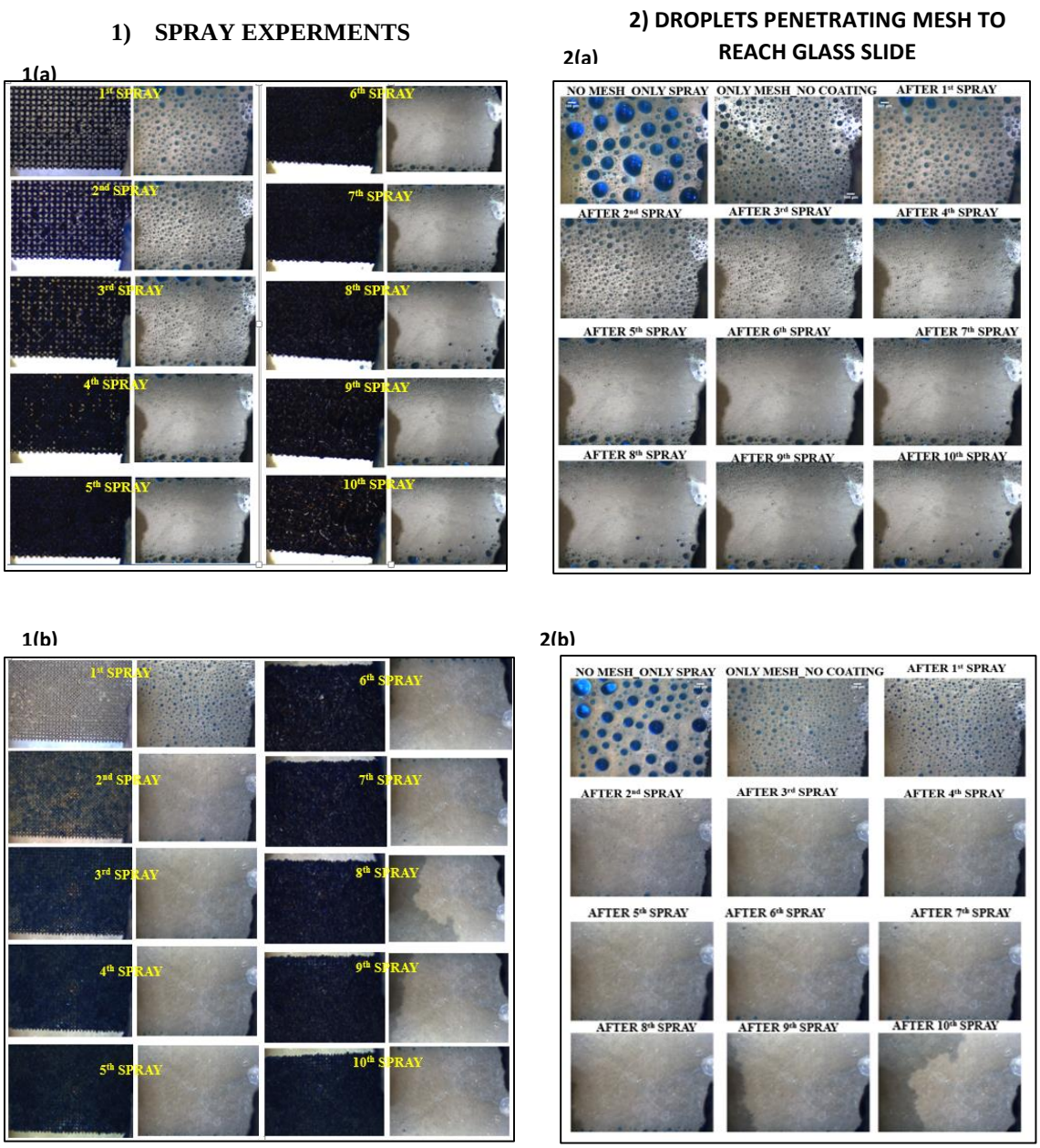

Figure 7.2 Spray Experiments Show the Amount of SAP Swelling on Mesh After Every Spray and the Area of Glass Slide Just Behind the Mesh is Shown Alongside Which Shows the Number of Droplets Penetrating the Mesh After Every Spray. 1(a) Shows the Spray Experiments on Coarser Mesh 60M (~230µm Opening, ~192µm Wire Diameter) and 1 (b) Shows on the Finer Mesh 100M (~140µm Opening, ~115µm Wire Diameter). The Summary of Droplets Penetrating the Mesh and Reaching the Glass Slide are Shown in 2. 2(a) Shows the Area of Glass Slide

It is evident from Figure 7.2 that the number and diameter of droplets reaching the glass slide placed behind the mesh sample keep decreasing with increasing number of sprays as the SAP on the mesh samples swells and blocks the water droplets hence confirming the effectiveness of self-sealing barrier formed. The difference in the results of fine and coarse mesh is evident from the Figure 7.2. Nearly all droplets are blocked after 4-5 sprays for coarser mesh 100M (~140µm opening) and for finer mesh 60M (~230µm opening), all drops are blocked after exposure to only 2-3 sprays cycles.

The results obtained from permeation experiments confirm the blockage effect of the proposed design for the self-sealing protective gear and can be recommended to be scaled to develop novel elastomers which will respond to the CWAs.

8. CONCLUSION

An alternative garment design that has the potential to overcome the drawbacks of existing MOPP apparel was proposed. Overall this design provides breathability through maintaining an open pore geometry until it is exposed to target chemicals such as CWAs. Once exposed, the pores close up due to the swelling of the garment polymer. This thesis explored the basic relation between the pore geometry, swelling properties of the polymer, and sealing effectiveness. First, PDMS coated stainless steel meshes were exposed to three solvents toluene, silicone oil, and acetone. It was found that in order to close completely, the pores would have to have initial ("open-state") diameters below 20 μm. Consequently, it was concluded that the polymer must have a significantly higher swelling ratio to allow for larger, more breathable, pores. To test this idea, water superabsorbing polymers (SAP) were tested. Uncontained SAP casted from liquid films was found difficult to handle once it turned into a gel state. To address this issue composites of SAP microparticles and elastomer (PDMS) were developed. Particles with three different size ranges were fabricated from a commercial sample through manual grinding and mesh sieving. The behavior of sessile water droplets on films as well as various woven stainless steel meshes with composites made with different particles was studied. It was found that the smallest size of the micro-particles (25 μm) was most effective at absorbing the water droplets because of a particle network effect that spread the liquid over large distances. As a result, highly desired sealing of pores away from the droplet position occurred. Aerosol permeation experiments demonstrated that the optimal designed sealed into an impermeable membrane after exposure to two short spray cycles. Naturally, current experiments demonstrate the basic feasibility of the proposed smart garment design. For

actual implementation, new superabsorbing polymers that selectively swell only with CWA, but not with water, need to be developed. This work shows that encapsulation of the SAP particles in an elastomer matrix could provide an interesting alternative to just simple polymer coatings.

REFERENCES

[1] B. S. Cadarette, S. N. Cheuvront, M. a Kolka, L. a Stephenson, S. J. Montain, and M. N. Sawka, "Intermittent microclimate cooling during exercise-heat stress in US army chemical protective clothing.," *Ergonomics*, vol. 49, no. 2, pp. 209–219, 2006.

[2] R. R. G. Thomas L. Endrusick, , Julio A. Gonzalez, "Improved comfort of US military chemical and biological protective clothing," Elsevier Ergon. B. Ser., pp. 369–373, 2005.

[3] K. B. P. Karen L. Speckman ∗, Anne E. Allan, Michael N. Sawka, Andrew J. Young, Stephen R. Muza, "Perspectives in microclimate cooling involving protective clothing in hot environments," *Int. J. Ind. Ergon.*, vol. 3, no. 2, pp. 121–147.

[4] J. Hu, H. Meng, G. Li, and S. I. Ibekwe, "A review of stimuli-responsive polymers for smart textile applications," *Smart Mater. Struct.*, vol. 21, no. 5, p. 053001, 2012.

[5] T.-S. Wong, S. H. Kang, S. K. Y. Tang, E. J. Smythe, B. D. Hatton, A. Grinthal, and J. Aizenberg, "Bioinspired self-repairing slippery surfaces with pressure-stable omniphobicity," *Nature*, vol. 477, no. 7365, pp. 443–447, 2011.

[6] C. Shillingford, N. MacCallum, T.-S. Wong, P. Kim, and J. Aizenberg, "Fabrics coated with lubricated nanostructures display robust omniphobicity.," *Nanotechnology*, vol. 25, p. 014019, 2014.

[7] D. P. Holmes and A. J. Crosby, "Snapping surfaces," *Adv. Mater.*, vol. 19, no. 21, pp. 3589–3593, 2007.

[8] J. L. Zhang, W. M. Huang, H. B. Lu, and L. Sun, "Thermo- / chemo-responsive shape memory / change effect in a hydrogel and its composites," vol. 53, pp. 1077–1088, 2014.

[9] L. Sun and W. M. Huang, "Thermo/moisture responsive shape-memory polymer for possible surgery/operation inside living cells in future," *Mater. Des.*, vol. 31, no. 5, pp. 2684–2689, 2010.

[10] B. Yang, W. M. Huang, C. Li, and L. Li, “Effects of moisture on the thermomechanical properties of a polyurethane shape memory polymer,” *Polymer (Guildf).*, vol. 47, no. 4, pp. 1348–1356, 2006.

[11] A. Lendlein and R. Langer, “Biodegradable, elastic shape-memory polymers for potential biomedical applications.,” *Science*, vol. 296, no. 5573, pp. 1673–6, 2002.

[12] Q. Meng, J. Hu, and L. Yeung, “An electro-active shape memory fibre by incorporating multi-walled carbon nanotubes,” *Smart Mater. Struct.*, vol. 16, pp. 830–836, 2007.

[13] H. Feil, Y. H. Bae, J. Feijen, and S. W. Kim, “Mutual influence of pH and temperature on the swelling of ionizable and thermosensitive hydrogels,” *Macromolecules*, vol. 25, no. 20, pp. 5528–5530, 1992.

[14] J. F. Mano, “Stimuli-responsive polymeric systems for biomedical applications,” *Adv. Eng. Mater.*, vol. 10, no. 6, pp. 515–527, 2008.

[15] H. Meng and G. Li, “A review of stimuli-responsive shape memory polymer composites,” *Polymer (Guildf).*, vol. 54, no. 9, pp. 2199–2221, 2013.

[16] W. M. Huang, Y. Zhao, C. C. Wang, Z. Ding, H. Purnawali, C. Tang, and J. L. Zhang, “Thermo/chemo-responsive shape memory effect in polymers: A sketch of working mechanisms, fundamentals and optimization,” *J. Polym. Res.*, vol. 19, no. 9, 2012.

[17] J. Leng, H. Lu, Y. Liu, W. M. Huang, and S. Du, “Shape-Memory Polymers—A Class of Novel Smart Materials,” *MRS Bull.*, vol. 34, no. 11, pp. 848–855, 2009.

[18] H. B. Lu, W. M. Huang, and Y. T. Yao, “Review of chemo-responsive shape change/memory polymers,” *Pigment Resin Technol.*, vol. 42, no. 4, pp. 237–246, 2013.

[19] W. M. Huang, Y. Zhao, J. L. Zhang, and H. B. Lu, “Chemo-responsive Shape Memory/change Effect in Polymeric Materials Based on Transport Phenomena,” *J. Fluid Flow, Heat Mass Transf.*, vol. 1, pp. 16–22, 2014.

[20] D. Bhanushali, S. Kloos, C. Kurth, and D. Bhattacharyya, “Performance of solvent-resistant membranes for non-aqueous systems: Solvent permeation results and modeling,” *J. Memb. Sci.*, vol. 189, no. 1, pp. 1–21, 2001.

[21] Lee, Park, and Whitesides, “Solvent compatibility of poly (dimethylsiloxane)-based microfluidic devices,” *Anal. Chem. Dc-*, vol. 75, no. 23, pp. 6544–6554, 2003.

[22] R. Dangla, F. Gallaire, and C. N. Baroud, “Microchannel deformations due to solvent-induced PDMS swelling.,” *Lab Chip*, vol. 10, no. 21, pp. 2972–2978, 2010.

[23] K. S. Koh, J. Chin, J. Chia, and C. L. Chiang, “Quantitative studies on PDMS-PDMS interface bonding with piranha solution and its swelling effect,” *Micromachines*, vol. 3, no. 2, pp. 427–441, 2012.

[24] J. C. McDonald, M. L. Chabinyc, S. J. Metallo, J. R. Anderson, A. D. Stroock, and G. M. Whitesides, “Prototyping of microfluidic devices in poly(dimethylsiloxane) using solid-object printing,” *Anal. Chem.*, vol. 74, no. 7, pp. 1537–1545, 2002.

[25] H. Becker and L. E. Locascio, “Polymer microfluidic devices,” *Talanta*, vol. 56, no. 2, pp. 267–287, 2002.

[26] H. Chen, X. Zhang, D. Zhang, J. Pan, and I. Hagiwara, “Large-scale equal-proportional amplification bio-replication of shark skin Based on solvent-swelling PDMS,” *J. Appl. Polym. Sci.*, vol. 130, no. 4, pp. 2383–2389, 2013.

[27] C. V. Rumens, M. A. Ziai, K. E. Belsey, J. C. Batchelor, and S. J. Holder, “Swelling of PDMS networks in solvent vapours; applications for passive RFID wireless sensors,” *J. Mater. Chem. C*, vol. 3, no. 39, pp. 10091–10098, 2015.

[28] L. E. M. Gevers, G. Meyen, K. De Smet, P. Van De Velde, F. Du Prez, I. F. J. Vankelecom, and P. A. Jacobs, “Physico-chemical interpretation of the SRNF transport mechanism for solutes through dense silicone membranes,” *J. Memb. Sci.*, vol. 274, no. 1–2, pp. 173–182, 2006.

[29] S. C. George and S. Thomas, “Transport phenomena through polymeric systems,” *Prog. Polym. Sci.*, vol. 26, no. 6, pp. 985–1017, 2001.

[30] J. S. Yoo, S. J. Kim, and J. S. Choi, “Swelling Equilibria of Mixed Solvent/Poly(dimethylsiloxane) Systems,” *J. Chem. Eng. Data*, vol. 44, no. 1, pp. 16–22, 1999.

[31] M. V Badiger, A. K. Lele, and M. G. Kulkami, “Swelling and Phase Transitions in Deforming Polymeric Gels,” *Ind. Eng. Chem. Res.*, vol. 33, no. 10, pp. 2426–2433, 1994.

[32] X. Zhu, G. Wu, R. Dong, C.-M. Chen, and S. Yang, “Capillarity induced instability in responsive hydrogel membranes with periodic hole array,” *Soft Matter*, p. -, 2012.

[33] J. H. Jang, C. Y. Koh, K. Bertoldi, M. C. Boyce, and E. L. Thomas, “Combining Pattern Instability and Shape-Memory Hysteresis for Phononic Switching,” *Nano Lett.*, vol. 9, no. 5, pp. 2113–2119, 2009.

[34] S. Willshaw and T. Mullin, “Pattern switching in two and three-dimensional soft solids,” *Soft Matter*, vol. 8, p. 1747, 2012.

[35] T. Mullin, S. Deschanel, K. Bertoldi, and M. C. Boyce, “Pattern transformation triggered by deformation,” *Phys. Rev. Lett.*, vol. 99, no. 8, pp. 1–4, 2007.

[36] Y. Zhang, E. A. Matsumoto, A. Peter, P. C. Lin, R. D. Kamien, and S. Yang, “One-step nanoscale assembly of complex structures via harnessing of an elastic instability,” *Nano Lett.*, vol. 8, no. 4, pp. 1192–1196, 2008.

[37] D.-Y. Khang, H. Jiang, Y. Huang, and J. A. Rogers, “A Stretchable Form of Single-Crystal,” *Science (80-.).*, vol. 311, no. January, pp. 208–212, 2006.

[38] S. Cai, K. Bertoldi, H. Wang, and Z. Suo, “Osmotic collapse of a void in an elastomer: breathing, buckling and creasing,” *Soft Matter*, vol. 6, no. May, p. 5770, 2010.

[39] X. Zhu, Y. Zhang, D. Chandra, S. C. Cheng, J. M. Kikkawa, and S. Yang, "Two-dimensional photonic crystals with anisotropic unit cells imprinted from poly(dimethylsiloxane) membranes under elastic deformation," *Appl. Phys. Lett.*, vol. 93, no. 16, pp. 1–4, 2008.

[40] W. Chen, R. H. W. Lam, and J. Fu, "Photolithographic surface micromachining of polydimethylsiloxane (PDMS).," *Lab Chip*, vol. 12, no. 2, pp. 391–5, 2012.

[41] L. P. Esteves, "Superabsorbent polymers: On their interaction with water and pore fluid," *Cem. Concr. Compos.*, vol. 33, no. 7, pp. 717–724, 2011.

[42] D. Snoeck, D. Schaubroeck, P. Dubruel, and N. De Belie, "Effect of high amounts of superabsorbent polymers and additional water on the workability, microstructure and strength of mortars with a water-to-cement ratio of 0.50," *Constr. Build. Mater.*, vol. 72, pp. 148–157, 2014.

[43] M. Zohuriaan-Mehr and K. Kabiri, "Superabsorbent polymer materials: a review," *Iran. Polym. J.*, vol. 17, no. 6, pp. 451–477, 2008.

[44] L. Wu, M. Liu, and Rui Liang, "Preparation and properties of a double-coated slow-release NPK compound fertilizer with superabsorbent and water-retention," *Bioresour. Technol.*, vol. 99, no. 3, pp. 547–554, 2008.

[45] W. A. Marlene Elizabeth Conway, "Soil additive in the form of a coating," WO 2001066668 A2, 2001.

[46] V. Mechtcherine, H.-W. Reinhardt, and (Eds.), "Application of Superabsorbent Polymers (SAP) in Concrete Construction: State-of-the-Art Report Prepared by Technical Committee 225-SAP," p. 164, 2012.

[47] V. Z. Detwiler, H. Celanese, M. Safety, D. Sheet, C. Corporation, M. Safety, D. Sheet, and P. Polyacrylate, "WATER SWELLABLE COATINGS AND METHOD OF MAKING SAME," 5,817,713, 1998.

[48] H. Lee, "Potential of superabsorbent polymer for self-sealing cracks in concrete," *Adv. Appl. Ceram.*, vol. 109, no. 5, pp. 296–302, 2010.

[49] L. (IT); T. A. S. C. M. Marco Serra, H. S. P. (US), M. (Us); J. Derry' NH (Us), Cleveland Arthur Heath, Medéld, I. (US) Edward Jarvls, Fort Wayne, and (73), "SEALING DEVICE FOR BODY SUIT AND SEALING METHOD USING HYDROGEL," US 7,313,829 B1, 2008.

[50] A. Borde, M. Larsson, Y. Odelberg, J. Hagman, P. L.wenhielm, and A. Larsson, "Increased water transport in PDMS silicone films by addition of excipients," *Acta Biomater.*, vol. 8, no. 2, pp. 579–588, 2012.

[51] S. Sakohara, F. Muramoto, and M. Asaeda, "Swelling and shrinking processes of sodium polyacrylate-type super-absorbent gel in electrolyte solutions," *Journal of Chemical Engineering of Japan*, vol. 23, no. 2. pp. 119–124, 1990.

[52] N. Dehbari and Y. Tang, "Water swellable rubber composites: An update review from preparation to properties," *J. Appl. Polym. Sci.*, vol. 132, no. 46, pp. 1–11, 2015.

[53] "Super-Absorbing Polymer Powder." [Online]. Available: https://www.cmu.edu/gelfand/k12-teachers/polymers/polymer-and-absorption/super-absorb-powder.html.

[54] G. K. Elyashevich, N. G. Bel'nikevich, and S. a. Vesnebolotskaya, "Swelling-contraction of sodium polyacrylate hydrogels in media with various pH values," *Polym. Sci. Ser. A*, vol. 51, no. 5, pp. 550–553, 2009.

[55] J. H. Park and D. Kim, "Preparation and Characterization of Water-Swellable," pp. 115–121, 2001.

[56] A. Lucantonio, L. Teresi, and A. Desimone, "Journal of the Mechanics and Physics of Solids Continuum theory of swelling material surfaces with applications to thermo-responsive gel membranes and surface mass transport," *J. Mech. Phys. Solids*, pp. 1–14, 2016.

[57] M. Definition, "MEMS Pressure Sensor Drift Due to Hygroscopic Swelling," no. Figure 1, pp. 1–28.

[58] N. Gershenfeld, "NMM:9 Finite Elements."